POWER OUTPUT MODELING AND OPTIMIZATION FOR A SINGLE AXIS TRACKING SOLAR FARM ON SKEWED TOPOGRAPHY CAUSING EXTENSIVE SHADING

A Thesis

presented to

the Faculty of California Polytechnic State University,

San Luis Obispo

In Partial Fulfillment

of the Requirements for the Degree

Master of Science in Mechanical Engineering

by

Logan Smith

June 2021

COMMITTEE MEMBERSHIP

TITLE:	Power Output Modeling and Optimization for a Single Axis Tracking Solar Farm on Skewed Topography Causing Extensive Shading
AUTHOR:	Logan Joseph Smith
DATE SUBMITTED:	June 2021
COMMITTEE CHAIR:	Jacques Belanger, Ph.D. P.E. Assistant Professor of Mechanical Engineering PG&E Professor of Nuclear and Renewable Energy
COMMITTEE MEMBER:	Andrew Davol, Ph.D. P.E. Professor of Mechanical Engineering
COMMITTEE MEMBER:	Dale Dolan, Ph.D. Professor of Electrical Engineering

ABSTRACT

Power Output Modeling and Optimization for a Single Axis Tracking Solar Farm on Skewed Topography Causing Extensive Shading

Logan Joseph Smith

Many utility-scale solar farms use horizontal single axis tracking to follow the sun throughout the day and produce more energy. Solar farms on skewed topography produce complex shading patterns that require precise modeling techniques to determine the energy output. To accomplish this, MATLAB was used in conjunction with NREL weather predictions to predict shading shapes and energy outputs. The MATLAB models effectively predicted the sun's position in the sky, panel tilt angle throughout the day, irradiance, cell temperature, and shading size. The Cal Poly Gold Tree Solar Farm was used to validate these models for various lengths of time. First, the models predicted the shading and power output for a single point in time. Four points of time measurements were taken; resulting in 6 to 32 percent difference in shade height, 5 to 60 percent difference for shade length, and 29 to 59 percent difference for power output. This shows the difficulty of predicting a point in time and suggests the sensitivity of numerous variables like solar position, torque tube position, panel tilt, and time itself. When predicting the power over an entire day, the power output curves for a single inverter matched almost exactly except for in the middle of the day due to possible inaccurate cell temperature modeling or the lack of considering degradation and soiling. Since the backtracking region of the power curve is modeled accurately, the optimization routine could be used to reduce interrow shading and maximize the energy output for a single zone of the solar field. By assuming every day is sunny, the optimization routine adjusted the onset of backtracking to improve the energy output by 117,695 kilowatt hours for the year or 8.14 percent compared to the nominal settings. The actual solar farm will likely never see this increase in energy due to cloudy days but should improve by a similar percentage. Further optimization of other zones can be analyzed to optimize the entire solar field.

ACKNOWLEDGMENTS

I would like to thank my family and friends for their support throughout the past five years. Without them, I would have never accomplished all that I have. I would also like to thank my advisors Dr. Belanger, Dr. Davol, and Dr. Dolan for providing me the guidance to complete this thesis. They created a supportive environment to analyze new ideas and always were excited to work with me.

TABLE OF CONTENTS

LIST OF TABLES viii

LIST OF FIGURES x

CHAPTER

1. INTRODUCTION 1

    1.1 Background 1

        1.1.1 Solar Energy 1

        1.1.2 Single Axis Tracking and Backtracking 2

    1.2 Objective 2

    1.3 Limitations 3

2. GOLD TREE SOLAR FARM SITE INFORMATION 4

    2.1 Solar Field Overview 4

    2.2 Panel Specifications 5

    2.3 Inverter Specifications 5

    2.4 Single Axis Tracker 5

    2.5 Green Power Monitor 6

3. MODELING 7

    3.1 Inputs 7

    3.2 Torque Tube Locations 7

    3.3 Solar Position 8

    3.4 Weather Predictions 9

    3.5 Tracking and Backtracking 9

    3.6 Irradiation 10

    3.7 Cell Temperature 12

    3.8 Shading 14

    3.9 Power 17

4. POINT IN TIME DATA MATCHING 19

    4.1 Data Collection Techniques 19

4.2 October 16th, 2020 Data Matching 21
4.2.1 Panel Tilt Angle 21
4.2.2 Shading Size 22
4.2.3 Inverter 55 Power Output 24
5. DAY DATA MATCHING 26
5.1 June 18th, 2020 26
5.2 January 16th, 2021 27
6. SENSITIVITY 29
6.1 Solar Position Models 29
6.2 Coordinate Sensitivity 29
6.3 Time Sensitivity 32
6.4 Panel Tilt Sensitivity 33
7. OPTIMIZATION OF POWER OUTPUT 34
7.1 Predicted Baselines 34
7.2 Optimization Methods 35
7.3 Optimized Energy 38
7.4 Splitting Zone Z1 and Y4 40
8. CONCLUSION AND FUTURE WORK 41
8.1 Conclusion 41
8.2 Future Work 42
REFERENCES 43
APPENDICES
A. Trina Solar Cell Datasheet 45
B. Yaskawa Inverter Data Sheet 47
C. Gold Tree Solar Farm Zoning and Torque Tube Coordinates 49
D. Optimization Routine MATLAB Code 53

LIST OF TABLES

Table Page

Table 4.1 Torque tube coordinates for the three rows connected to inverter 55 and row 540 which shades the first row in the afternoon. All coordinates are in feet. 19

Table 4.2 POA irradiance, tracking angle, and cell temperature data for October 16th, 2020. POA irradiance was found using the power from inverter 52. The tracker angle is the angle outputted by the GPM for the set panel tilt. The cell temperature was measured using an infrared thermometer on the back of the panels. 21

Table 4.3 Modeled panel angle vs actual panel angle at four different times on October 21st, 2020, for each row connected to inverter 55. The actual panel angle is larger than the modeled panel angle and has fluctuations that do not occur in the model. 22

Table 4.4 Modeled shade vs actual shade at four different times on October 21st, 2020 for each row connected to inverter 55. The modeled shade is found using the measured angles of the panels and is consistently an overestimate of the actual shade. 24

Table 4.5 Modeled power vs actual power at four different times on October 21st, 2020 for inverter 55. The actual power outputted is consistently higher than the modeled power and is around 30% higher for three out of four times. 25

Table 6.1 Varying sun elevation models and their effect on shading for October 16th, 2020 at 3:45 pm. The PVLib Equation was chosen to model the location of the sun in the sky. It matched the SunCalc.org online calculator and is within less than half a degree of the other models except the Seinfeld model. The height of shade for row 541 is also shown and how it decreases with increasing elevation angle. 29

Table 7.1 Unshaded and shaded energy predictions for each month assuming it is always sunny. Both predictions use a torque tube spacing of 11 ft, but the unshaded prediction assumes no interrow shading. This provides a maximum amount of energy that could theoretically be produced if the field was perfectly flat. The shaded energy predictions account for the shading and are then compared to the theoretical maximum as a percentage. 34

Table 7.2 Optimized west and east torque tube spacings for each month. The west torque tube spacings are large in the summer while the east torque tube spacings are larger in the winter. 37

Table 7.3 Optimized energy and its comparisons to the theoretical maximum and the nominal monthly energy assuming every day is sunny. The optimized energy is typically between 91 to 95% of the theoretical max for each month and about a 6 to 9% increase from the energy if the torque tube spacing was set to 11 feet. 38

Table 7.4 Optimized energy s for splitting Z1 and Y4. The original and new configuration of switching 6 rows from Z1 to Y4 are shown as well as the energy and percent increase. 40

Table C.1 Zone name and number of rows for the Gold Tree Solar Farm 50

Table C.2 Coordinates for the torque tubes in Zone Z1. The north end of Row 524 is taken to be the origin and Row 523 is a part of Zone Y4 but shades the first row of Z1 in the afternoons, so its coordinates are also included. All coordinates are in units of meters. 51

Table C.3 Coordinates for the torque tubes in Zone Y4. The north end of Row 504 is taken to be the origin. Row 524 is a part of Zone Y4 but shades the last row of Y4 in the mornings, so its coordinates are also included. Rows 501 to 503 are not included as they are not full length, and this analysis does not account for half or three-quarter length rows. All coordinates are in units of meters. 52

LIST OF FIGURES

Figure Page

Figure 1.1 Solar installation predictions as provided by Wood Mackenzie [1]. As can be seen, many utility-scale "front-of-the-meter" solar farms are predicted to be installed in the coming years..... 1

Figure 1.2 Effect of backtracking on shading: (a) shows the shading with no backtracking and (b) shows the elimination of the shading when backtracking is used. A side profile of the panels is shown where the blue is the panel itself and the yellow represents the sunlight hitting the panels. The black rectangle shows how the first row shades the following row..... 2

Figure 2.1 The Gold Tree Solar Farm 4

Figure 3.1 Aerial view of torque tubes with superimposed modeled locations. The red modeled torque tubes line up well with the satellite imagery. 8

Figure 3.2 Apparent solar elevation for December 21st and June 21st. *pvl_ephemeris* shows that the sun elevation is highest in the summer months but still parabolic in shape. The time of day in June does not account for daylight savings. 9

Figure 3.3 Panel tilt for Zone Z1 on January 1st, 2021 comparing the model to actual angle data. Two modified tube spacing settings are shown: one at 9.51 ft and one at 11 ft. On this day, the actual morning setting is set to 11ft and the actual afternoon setting is set to 9.51 feet. The data closely matches that of the model though the model predicts the sunrise to be slightly earlier. 10

Figure 3.4 POA Irradiance predicted by the model verified against real-world data for January 16th, 2021 and July 12th, 2020 data. For a clear day, the model accurately predicts the amount of POA irradiance expected in the winter and the summer. 12

Figure 3.5 Cell temperature and ambient temperature throughout the day on January 16th, 2021. The cell temperature and ambient temperature match until the sun rises. The added irradiation causes the cell temperature to rapidly climb by roughly 20 °C and continue to climb throughout the day until the sun begins to set. 14

Figure 3.6 Shading patterns and dimensions. Typically, the shading seen is in the shape of a triangle or a trapezoid that extends the length of the panels. Both shapes can also be shifted from the left or right edge of the panel leaving an unshaded gap. 15

Figure 3.7 Solar coordinates view of a shaded row looking down the z' axis. The blue outlined shape is the projected row in front where the solid blue shape is the row being shaded. The triangle where the two panels overlap is the shading shape. 16

Figure 3.8 Shading for Z1 on June 21st at 7 pm. All 26 rows of Z1 are shown as well as the last row of the neighboring zone. Yellow corresponds to panels that are seeing sun where the black is the shading pattern. The gradient shape represents the uneven ground. Several rows on the east side are substantially shaded due to the decrease in ground elevation. 16

Figure 3.9 Solar panel schematic with diodes and substrings. If one substring loses power due to shading, the diode can bypass it. 17

Figure 3.10 Percent of power versus percent shading on the bottom cell of the substring. As the shading begins to the cover the bottom cell, the power in the substring and panel begin to decrease linearly. At 30% shaded, the bottom cell fails to produce current, and the substring stops producing power. The other 2 substrings can continue to produce power in the panel. 18

Figure 4.1 Inverter 55 and 52 locations at the Gold Tree Solar Farm. Inverter 55 is the inverter being analyzed and inverter 52 is used as an unshaded reference. Inverter 55 is connected to rows 541 through 543. Row 540 shades the first row of inverter 55 in the afternoon. 20

Figure 4.2 Actual shading seen at the Gold Tree Solar Farm. The shade shape is a triangle extending across the row. As time passes, this triangle grows in area. 23

Figure 5.1 Modeled vs actual power out of inverter 55 for June 18th, 2020. The modeled power and actual power closely match including in the morning and afternoons when backtracking is occurring. The power level caps at around 60 kW due to the inverter's continuous power rating. 26

Figure 5.2 Modeled vs actual power out of inverter 55 for January 16th, 2021. The highest line is the pure model prediction for power. The next two highest lines are the power predicted using GPM data for POA irradiance and ambient temperature where the lower line also includes a 3% soiling factor. The bottom line is the actual power outputted by the inverter. All lines are relatively effective at predicting the backtracking region but are higher during the middle of the day during peak power generation. 27

Figure 5.3 Modeled vs actual POA irradiance for January 16th, 2021. The actual POA irradiance is measured from a different zone but the overall shape and size of the two curves are very close to each other. 28

Figure 6.1 Change in x-coordinate of row 541 and its effect on the height and length of the shade. A one-inch change in the x-coordinate causes a .01-inch increase in height and a .63-inch decrease in length. 30

Figure 6.2 Change in y-coordinate of row 541 and its effect on the height and length of the shade. A one-inch change in the y-coordinate causes a .58-inch decrease in height and a 11.0-inch decrease in length. 31

Figure 6.3 Change in z-coordinate of row 541 and its effect on the height and length of the shade. A one-inch change in the z-coordinate causes a 1.46-inch decrease in height and a 28.21-inch decrease in length. 31

Figure 6.4 Height of shade and elevation angle change over five minutes for October 16th, 2020. Over five minutes, the height of the shading on rows 541, 542, and 543 increases by more than 2.5 inches. The sun elevation decreasing by almost a degree causes this increase in shading. 32

Figure 6.5 Height of shade for change in panel tilt of row 541. Row 541's shade increases by .615 inches per degree. Row 542 shading is also shown and increases by .842 inches per degree. 33

Figure 7.1 Monthly energy vs west torque tube spacing for January. As the torque tube spacing was varied, the monthly energy curve was created. The maximum monthly energy occurred just above 9 feet. 35

Figure 7.2 Refined monthly energy vs west torque tube spacing for January. The maximum monthly energy occurs at a west torque tube spacing of 9.07 feet. 36

Figure 7.3 Optimization curves and nominal energies for each month. All the curves are normalized to the theoretical maximum energy. Each curve shows the shape of the optimization and where the maximum point is. All curves are based only on the west torque tube spacing optimization. 37

Figure 7.4 Nominal shaded energy, optimized energy, and theoretical maximum energies for each month. The optimized energy is approximately halfway between the nominal and maximum energies. 39

Figure 7.5 Percent area shaded on panels for December 21st and June 21st, 2021 for different modified torque tube spacings. The higher the modified torque tube spacing, the more shading there is throughout the day. The optimized value is not the minimum amount of shading but instead a balance between shading and POA irradiance 39

Chapter 1

INTRODUCTION

1.1 Background

1.1.1 Solar Energy

As the energy sector moves toward renewables to curtail carbon emissions, more solar farms are being designed and installed. To produce more energy per acre of land, these solar farms are using single axis tracking to track the sun throughout the day. Figure 1.1 shows the predicted solar installations for the US in the coming years as predicted by Wood Mackenzie [1]. With the predicted increase in solar farm installations, many will likely not be on perfectly flat land due to expenses and availability. Knowing how the skewed topography affects energy production severely impacts the design and construction of these solar farms. More accurate predictions of the energy generation will allow for these systems to have an even greater influence on the grid and avoid brownouts when insufficient energy is generated. This thesis focuses on the modeling techniques and analysis of the utility-scale Gold Tree Solar Farm located at Cal Poly and the optimization of its energy output.

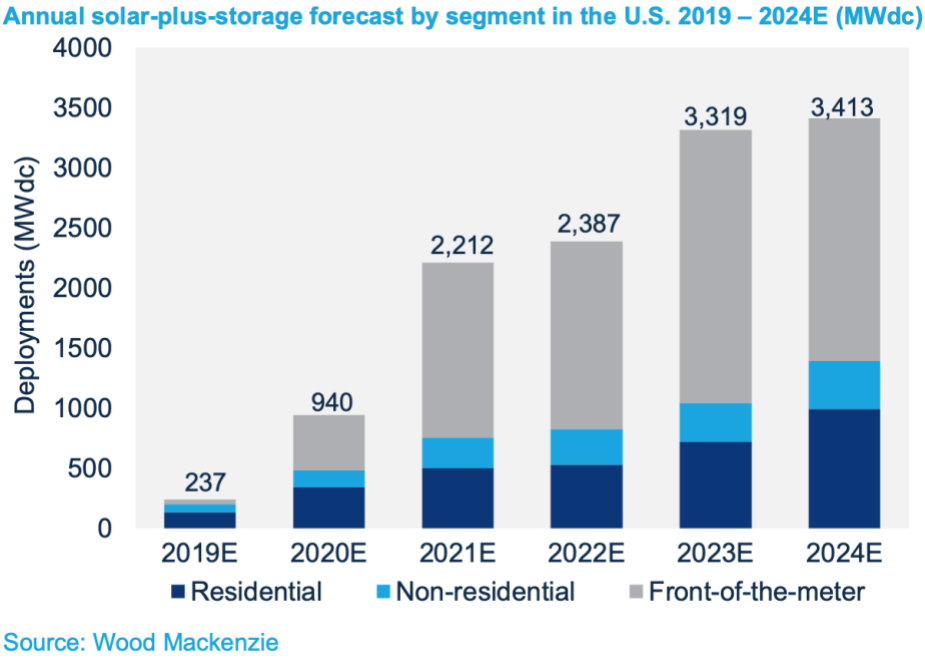

Figure 1.1 Solar installation predictions as provided by Wood Mackenzie [1]. As can be seen, many utility-scale “front-of-the-meter” solar farms are predicted to be installed in the coming years.

1.1.2 Single Axis Tracking and Backtracking

To improve the energy output of a solar farm, horizontal single axis tracking (HSAT) is often used since the expenses are outweighed by the increase in energy production. By using HSAT, the panels can produce more energy by tilting the panels towards the sun; however, when the sun is lower in the sky, a row of panels can often shade the row behind them. Even small shading of solar panels has a large effect on energy production. To combat this effect, backtracking is used. Backtracking algorithms use the row spacing and panel width to find the optimal angle which produces the most energy and prevent shading [2]. When backtracking, the solar irradiation is no longer perpendicular to the panels, lowering the energy produced. Figure 1.2 shows how the irradiation and shading are affected by backtracking. When the sun is low in the sky, the panels tilt to be more parallel to the ground to avoid shading the row behind them. Balancing the perpendicular irradiance with shading allows for the highest amount of energy to be produced by the solar farm. The algorithm used in these tracking systems assume that the ground is flat or sloped in a single direction. But in the case of skewed topography, the shading can cause severe energy generation losses.

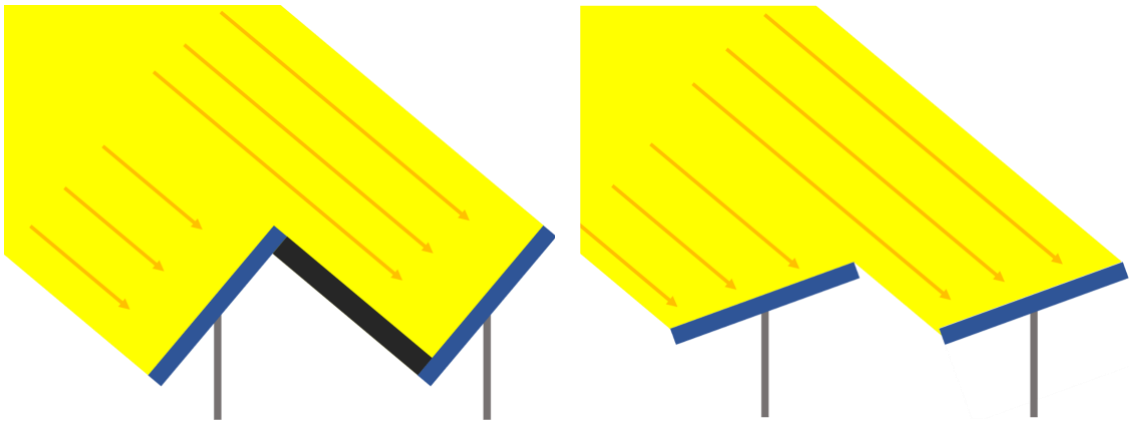

(a) (b)

Figure 1.2 Effect of backtracking on shading: (a) shows the shading with no backtracking and (b) shows the elimination of the shading when backtracking is used. A side profile of the panels is shown where the blue is the panel itself and the yellow represents the sunlight hitting the panels. The black rectangle shows how the first row shades the following row.

1.2 Objective

The purpose of this thesis is to model and optimize one of the twelve zones of the Gold Tree Solar Farm by predicting the shading between rows and modifying the control algorithm of the tracking systems to maximize the energy output. The as-built solar farm is producing less energy than predicted due to the

inadequate consideration of the skewed topography. The backtracking algorithms used consider the ground to be sloped in only a single direction causing much more interrow shading than predicted. This thesis first discusses how backtracking affects energy generation, then describes the modeling process used to predict irradiance, cell temperature, and shading to find the power output for each row at the solar farm. Using real-world data, this model was then verified, and the sensitivity of various variables was analyzed. The sensitivity analysis provides a basis for how to model other solar farms and how precise measurements are necessary to predict actual energy generation. The thesis concludes with an optimization that increases the energy generation from one of the worst zones at the solar farm. By describing the modeling and optimization processes, this thesis provides a general roadmap for optimizing other zones of the Gold Tree farm and other solar farms on skewed topography that use single axis tracking.

1.3 Limitations

All the solar models used for data matching assume sunny days with typical year values for ambient temperature. The optimized energies are not reflective of real-world data and therefore should not be used for predictions of energy output. The model is also not effective at predicting power output for a single inverter at a single point in time due to inaccuracies in data collection and sensitivity of several geometric and weather variables. It is also important to note that the current model cannot accurately predict cell temperature given the weather station measured wind speed. The wind speed cools down the cells but it is difficult to account for due to the complexity of the air flow around multiple rows of panels in this skewed topography.

Chapter 2

GOLD TREE SOLAR FARM SITE INFORMATION

2.1 Solar Field Overview

The optimization and modeling of the energy output were all based on the Gold Tree Solar Farm located at Cal Poly in San Luis Obispo. This installation has a nominal power rated output of 4.5MW and an expected yearly energy generation of approximately 11 million kWh. However, the unexpected shading caused a reduction in the actual energy generated. The solar farm was designed by REC Solar and provides power and research opportunities to Cal Poly. To produce energy, the solar farm utilizes two different types of panels: half-cut and full-cut. The zone under analysis for this optimization contains only the full-cut solar panels. The panels are found in various zones with up to 26 rows. Each row is typically spaced 11 feet apart to limit the amount of shading and is along the north-south direction. To position the panels to face the sun throughout the day and increase energy, the solar farm uses horizontal single axis tracking (HSAT). Each zone is controlled by a separate tracker that allows the settings to be changed for each of the twelve zones individually. Figure 2.1 shows the Gold Tree Solar Farm as well as the hills that the panels were constructed on. This uneven ground causes irregular shading which is the driving force behind the following analysis and optimization of the energy output.

Figure 2.1 The Gold Tree Solar Farm

2.2 Panel Specifications

All the panels used in this analysis are Trina Tallmax Plus monocrystalline modules. These panels have 72 cells connected in three substrings, have an efficiency of 17.8 percent, and a peak power output of 345 Watts. Each substring has 24 cells that are connected in series in columns of 12 cells. The substrings have diodes that allow for a specific substring to be bypassed if it is shaded. Since there are three substrings, shading a single cell in a substring can cause a third of the panel to stop producing power. This specific panel is used for half of the solar farm. The other half of the solar farm uses half-cut panels which are less affected by shading due to their more sectional design [3]. Therefore, this type of panel is not analyzed for this optimization. The datasheets for the Trina Solar panels can be found in Appendix A.

2.3 Inverter Specifications

All the inverters at the solar farm are Yaskawa Solectria 60TL string inverters. These inverters convert the DC power from the panels to three-phase AC power at 480 VAC. They have a CEC efficiency of 98.5 percent and output a maximum 60 kilowatts of power. The inverters have three maximum power point tracking (MPPT) controllers that determine the optimum point on the current-voltage curve. Each of the MPPT controllers is attached to four strings in parallel. Each of these strings is composed of 19 panels in series. Having three MPPT controllers allows the inverter to maximize the amount of power outputted even when shading occurs on part of the row. The full datasheet for these inverters can be seen in Appendix B.

2.4 Single Axis Tracker

The panels at the solar farm are connected to motors which control the pitch of the rows to point at the sun. Each motor is connected to no more than 26 rows and controls each row simultaneously. This splits the field into 12 different zones as seen in Appendix C. The zone with persistent shading and the subject of this analysis is zone Z1. The trackers used are developed by Array Technologies and can tilt the panels from -52° to 52° as well as backtrack when needed.

The Gold Tree Solar Farm uses a backtracking algorithm which adjusts the onset of backtracking. by inputting the tube spacing parameter in the software. The software allows for different tube spacing

parameters to be input for morning and evening. By modifying the tube spacing in the control algorithm the energy output can be optimized. Backtracking at the optimum time is necessary to reduce shading while keeping the panels tilted towards the sun as much as possible. Since the terrain is skewed in both the North-South and East-West directions, the current backtracking model is unable to accurately predict the optimal modified tube spacing and thus an optimization routine is needed.

2.5 Green Power Monitor

While modeling the solar farm, data is required to validate the power outputs. The Green Power Monitor (GPM) provides real-time data for the solar farm [4]. Power output, POA irradiance, ambient temperature, and wind speed can all be exported from the GPM. This database provides information for every five minutes and is stored online to be used for verification.

Chapter 3

MODELING

MATLAB was used to model the Gold Tree Solar Farm and predict the energy output of several subsections of the array. This code was then used to optimize the energy output by modifying the backtracking parameters. To predict the energy effectively, several inputs including date and time, coordinates for the panels, and modified tube spacings were needed as well as models for the solar position, weather, backtracking, irradiation, cell temperature, and shading on the panels.

3.1 Inputs

The code takes in various inputs to accurately model the solar field for different conditions. First, the start and end date-times are inputted. For this analysis, the maximum length of time is a month and the shortest is a single point in time. If the time crosses a change in daylight savings, the date for this shift can also be included. Then, the time step for how often the model predicts the power output can be adjusted. Next, the coordinates of the end of the torque tubes are loaded. These coordinates are orientated with the x value in the north to south direction, the y value in the west to east direction, and the z value in the vertical direction. The modified tube spacing for the backtracking algorithm is then inputted along with the panel sizing and offset from the end of the torque tube. Finally, the location of the solar farm is inputted including latitude, longitude, and altitude.

3.2 Torque Tube Locations

The panels at the Gold Tree Solar Farm are connected to torque tubes that allow them to track the sun throughout the day. To model the field, the coordinates for the ends of these torque tubes were measured. A Leica DISTO S910 laser system was used to determine the x, y, and z coordinates of the ends of these torque tubes. This provided accurate modeling of the as-built field to then be analyzed. Figure 3.1 shows an aerial view of the solar field with the modeled torque tubes overlayed. As can be seen, zone Z1 is precisely modeled to within a few inches. The coordinates were measured multiple times using the laser system to provide locations within half an inch. In the future, a LIDAR system could be used to validate and create an even more accurate model of the torque tube locations for the whole field.

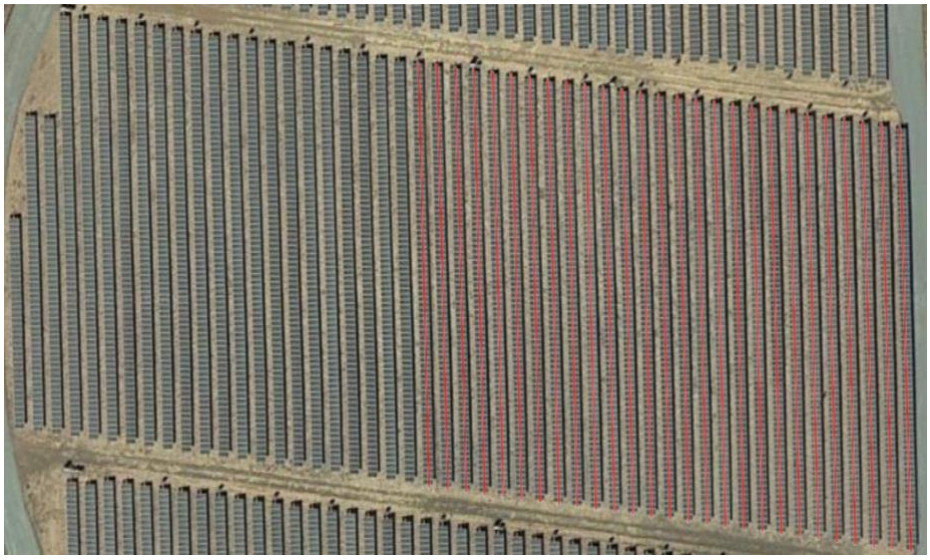

Figure 3.1 Aerial view of torque tubes with superimposed modeled locations. The red modeled torque tubes line up well with the satellite imagery.

3.3 Solar Position

Using the date and time, the position of the sun can be determined using the PVLib function, *pvl_ephemeris* [5]. This function outputs the azimuth, elevation, apparent elevation, and solar time. For the optimization, sun azimuth and apparent sun elevation are used. The apparent sun elevation differs from the sun elevation by considering the refraction caused by the atmosphere. More accurate solar positions can be outputted by including pressure and temperature; however, for this model, a standard 1 atm and 12° C was used. Figure 3.2 shows the apparent solar elevation output of this function for December 21st and June 21st. Since the elevation of the summer months is higher, it is expected that the solar farm will produce more energy during these months.

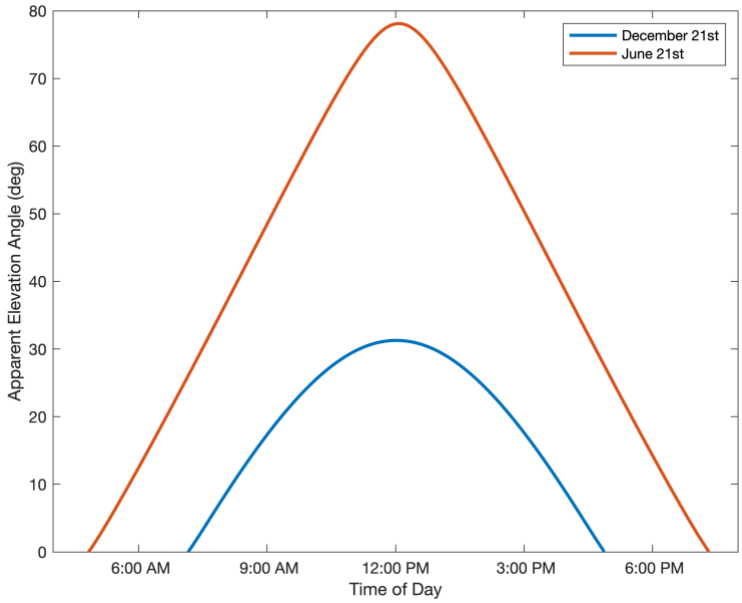

Figure 3.2 Apparent solar elevation for December 21st and June 21st. *pvl_ephemeris* shows that the sun elevation is highest in the summer months but still parabolic in shape. The time of day in June does not account for daylight savings.

3.4 Weather Predictions

The energy output for the solar cells is dependent on the cell temperature. This temperature is related to the ambient temperature, irradiance, and wind speed. For the optimization analysis, these parameters were taken from a typical meteorological year provided by the National Renewable Energy Laboratory (NREL). The data is taken over several years and each month represents a typical month at a certain location. Additionally, this data includes the different types of irradiances, the dry-bulb ambient air temperature, and the wind speed. When validating the model with real-world data, the ambient temperature, irradiance, and wind speed can be imported from the GPM to predict the cell temperature more accurately at the site.

3.5 Tracking and Backtracking

Since the Gold Tree Solar Farm uses single-axis tracking, a model was created to predict the panel tilt angle throughout the day. Tracking the sun increases the energy output of the panels but potentially causes shading in the early morning and late afternoon. During these times, the panels backtrack to reduce the shading (see section 3.8). The trackers used at the solar farm allow for a modified tube spacing to be inputted

for the morning and afternoon [2]. A lower tube spacing will cause the panels to backtrack for more of the day as seen in Figure 3.3 where the panel tilt angle is plotted for January 1st, 2021. When the modified tube spacing is 9.51 feet instead of 11 feet, the panels are backtracking later into the morning and earlier in the afternoon. The solar farm's actual tube spacing for zone Z1 is approximately 11 feet. Figure 3.3 also shows the panel tilt angle outputted by the GPM which closely matches the model. For this day, the morning modified tube spacing was set to 11 feet then changed to 9.51 feet in the afternoon. The model effectively predicts the backtracking and tracking regions, but is predicting the sunrise to be about five minutes earlier than the GPM shows. This variance could be attributed to the GPM outputting data at slightly different times as well as the panels' inability to move from -52 degrees to 0 degrees instantaneously.

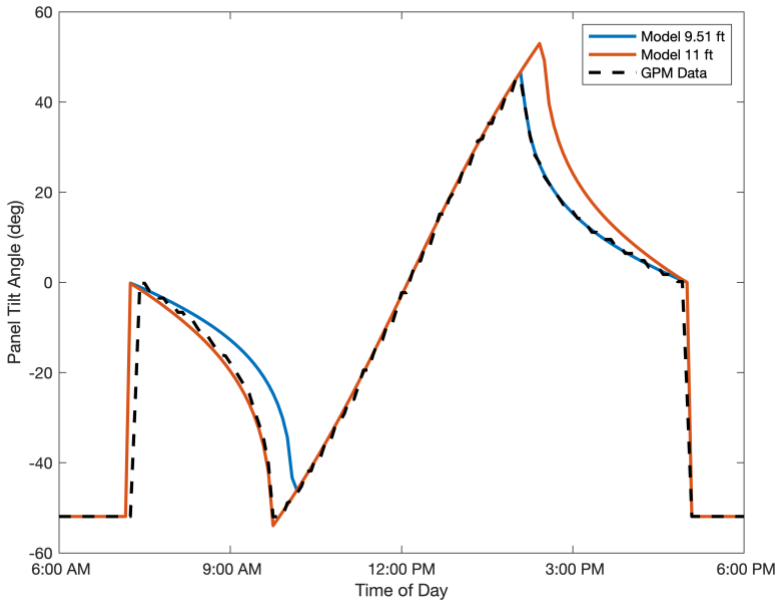

Figure 3.3 Panel tilt for Zone Z1 on January 1st, 2021 comparing the model to actual angle data. Two modified tube spacing settings are shown: one at 9.51 ft and one at 11 ft. On this day, the actual morning setting is set to 11ft and the actual afternoon setting is set to 9.51 feet. The data closely matches that of the model though the model predicts the sunrise to be slightly earlier.

3.6 Irradiation

The power outputted by the panels is directly related to the point of array (POA) irradiance. When analyzing a specific point in time or a specific day, the actual POA from the GPM can be inputted. However, for the optimization, the POA irradiance needs to be accurately predicted. To predict the POA irradiance,

PVLib's function *pvl_clearsky_ineichen* is used to find the global horizontal irradiance (GHI), diffuse horizontal irradiance (DHI), and direct normal irradiance (DNI) values for a given time and location [6]. These irradiances are used to find different parts of the POA irradiance. POA irradiance is defined as follows:

$$POA = POA_{dir} + POA_{diff,refl} + POA_{diff,sky}$$

where POA_{dir} is the irradiance from the ray of light, $POA_{diff,refl}$ is the light reflected off the ground, and $POA_{diff,sky}$ is the diffuse irradiance from the sky.

POA_{dir} is calculated using the DNI value found and the angle of incidence (AOI). The angle of incidence is found using PVLib's function *pvl_getaoi* which requires the panel tilt and the sun position. The POA_{dir} component can be then calculated as follows:

$$POA_{dir} = DNI \cdot \cos(AOI)$$

Next, the $POA_{diff,refl}$ component is calculated using the GHI value found, the reflectivity of the ground surface (or albedo), ρ, and the panel tilt, β. The reflectivity of the ground is assumed to be 0.2 [7].The equation to find the $POA_{diff,refl}$ is:

$$POA_{diff,refl} = GHI \cdot \rho \frac{1 - \cos(\beta)}{2}$$

Finally, the $POA_{diff,sky}$ is found using the *pvl_haydavies1980* function from PVLib [8]. This function requires the panel tilt angle, DHI, DNI, sun location, and the extraterrestrial solar radiation found using the *pvl_extraradiation* function from PVLib [9]. Once all the components are calculated, they are added together to find the total POA irradiance.

The modeled POA irradiance and the actual POA irradiance seen at the solar farm on January 16th, 2021 and July 12th, 2020 can be seen in Figure 3.4. These dates were selected since they represent two extremes during the year and are sunny days. The model is effective in predicting the POA irradiance on these days and small discrepancies seen can be attributed to many factors affecting irradiance, most likely humidity in this case. With higher humidity, the transmissibility of the air lowers and less solar radiation hits the panel. The model is unable to account for or predict the humidity of the air on a certain date. For the overall optimization, the model is suitable for predicting the POA irradiance. On the other hand, if actual power production is desired, the model can use the NREL data to predict the POA irradiance similar to the ambient temperature and wind speed.

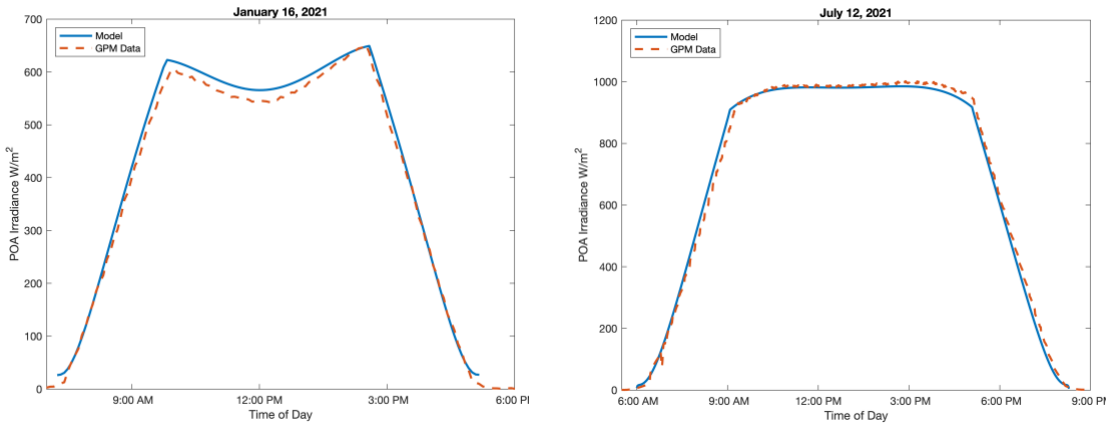

Figure 3.4 POA Irradiance predicted by the model verified against real-world data for January 16th, 2021 and July 12th, 2020 data. For a clear day, the model accurately predicts the amount of POA irradiance expected in the winter and the summer.

3.7 Cell Temperature

The energy generated by solar panels is heavily influenced by the temperature of the cell. Higher temperatures cause the energy to decrease and on sunny days, the panels can be much hotter than the ambient temperature. To predict the cell temperature a model proposed by Mattei et al. was used [10]. This model came from a comparative analysis by Schwingshackl et al. and is summarized here [11].

First, the energy absorption, I_a, for a panel is based on the irradiance, I, the transmittance of the panel, τ, and the absorptivity of the panel, α and was determined using the following equation.

$$I_a = \tau \alpha I$$

The value used for $\tau \alpha$ was 0.9 for this analysis, as recommended by Schwingshackl et al and I is the POA irradiance previously calculated in Section 3.6.

The amount of energy that is then converted to electrical energy, I_e, is based on the efficiency of the cell η_c and is given by:

$$I_e = \eta_c I_a$$

The efficiency of the panel is based on the cell temperature, T_c, the panel efficiency at standard conditions, η_{STC}, the temperature coefficient of maximal power at standard conditions, β_{STC}, and the temperature at standard conditions, T_{STC}. The equation for cell efficiency is as follows:

$$\eta_C = \eta_{STC}[1 - \beta_{STC}(T_c - T_{STC})]$$

where $\eta_{STC} = .178$ and $\beta_{STC} = .39\%/K$ for the cells under analysis, and $T_{STC} = 25℃$ as listed in Appendix A for the Trina Tallmax Plus cells.

Knowing the energy absorption into the cell and the energy converted to electricity, the heat can be equated to all the energy absorbed that is not being converted to electricity using an energy balance. The heat is assumed to be predominantly convection so the energy balance can be written as:

$$U_{PV}\,(T_c - T_a) = I\tau\alpha - I\eta_{STC}[1 - \beta_{STC}(T_c - T_{STC})]$$

where U_{PV} is the convection coefficient and T_a is the ambient temperature.

Solving for the cell temperature, T_c, the equation becomes:

$$T_c = \frac{U_{PV}\,T_a + I\,[\tau\,\alpha - \eta_{STC}(1 + \beta_{STC}T_{STC})]}{U_{PV} - \beta_{STC}\,\eta_{STC}\,I}$$

The convection coefficient, U_{PV}, can be then be obtained by

$$U_{PV} = a + b\,v_w$$

where v_w is the wind speed in meters per second, and a and b can be found using experimental data or the conditions provided by the manufacturer. For this analysis, a was 26.6 and b was 2.3 which was recommended by Mattei et al. Further experimentation is needed to validate these coefficients.

Figure 3.5 shows the cell temperature and ambient temperature throughout the day on January 21st, 2021 (a sunny day). At night, the ambient and cell temperature are the same; however, as the sun rises and the POA irradiance increases, the cell temperature climbs sharply and diverges from the ambient temperature. Throughout the day, the cell temperature continues higher than the ambient temperature until the sun begins to set. The actual cell temperature during the day greatly affects the amount of power the cells can output, and accurate modeling is required for precise power prediction.

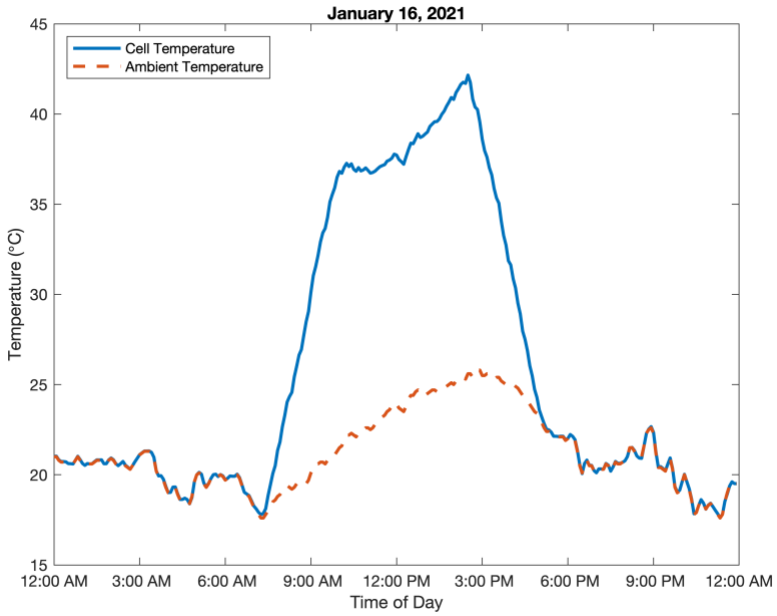

Figure 3.5 Cell temperature and ambient temperature throughout the day on January 16th, 2021. The cell temperature and ambient temperature match until the sun rises. The added irradiation causes the cell temperature to rapidly climb by roughly 20 °C and continue to climb throughout the day until the sun begins to set.

This model has some limitations. When a panel is shaded and there is no current flow, all the energy is converted to heat but for this temperature analysis, the panels are assumed to never be shaded. This is not the case for the Gold Tree Solar Farm, but shading occurs during the lower POA irradiation parts of the day, so the temperature model is not as severely affected. Also, further experimental data needs to be taken at the solar farm to validate the coefficients used to find the convection coefficient. Since there is a number of rows, the wind on each of them is likely not consistent with the overall wind speed and thus, the coefficients may fluctuate from row to row. Because of this, the power prediction models assume a constant wind speed of 1 meter per second to better match the actual power produced at the farm. This is also the wind speed that Mattei et al based their analysis on.

3.8 Shading

At the Gold Tree Solar Farm, the rows of panels are on uneven ground. This skewed topography causes various shading patterns on the panels that need to be accurately modeled to predict the power output. Figure 3.6 shows the common shapes of shading experienced by the panels. These shading patterns can be characterized by two shade heights, a shade length, and a shade shift.

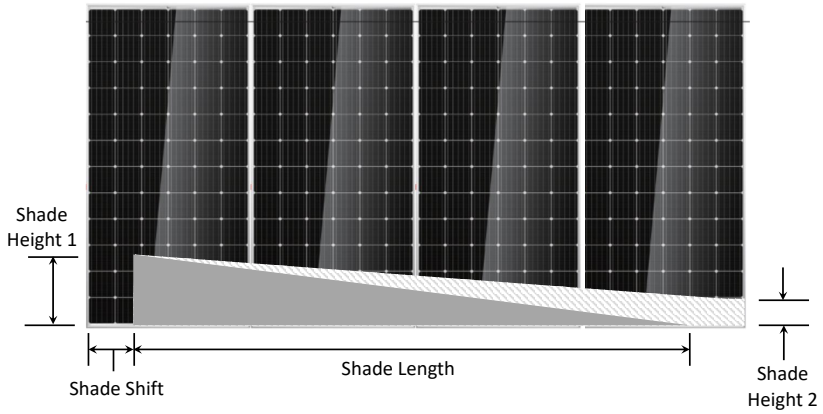

Figure 3.6 Shading patterns and dimensions. Typically, the shading seen is in the shape of a triangle or a trapezoid that extends the length of the panels. Both shapes can also be shifted from the left or right edge of the panel leaving an unshaded gap.

To accurately predict shading, the panel locations, sun location, and panel tilt were used to project the vertices of the panels onto the next row in the direction of the sun's rays. To accomplish this, the first panel's vertices are converted to a coordinate system where the z'-axis is pointing towards the sun. Looking at the new x'-y' plane created, the intersections between the panels can be found as seen in Figure 3.7 where the overlapping portion shown is the shape of the shading. After finding the shading shape, the intersection points are converted to a local panel coordinate system to be used in the power subroutine. These points are also converted back to the global coordinate system for graphical validation of the shading. This procedure was repeated for all subsequent rows.

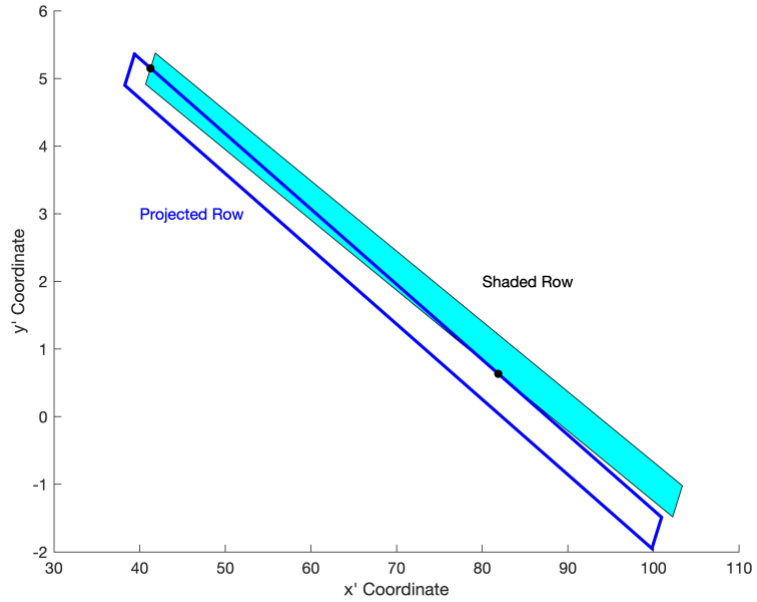

Figure 3.7 Solar coordinates view of a shaded row looking down the z' axis. The blue outlined shape is the projected row in front where the solid blue shape is the row being shaded. The triangle where the two panels overlap is the shading shape.

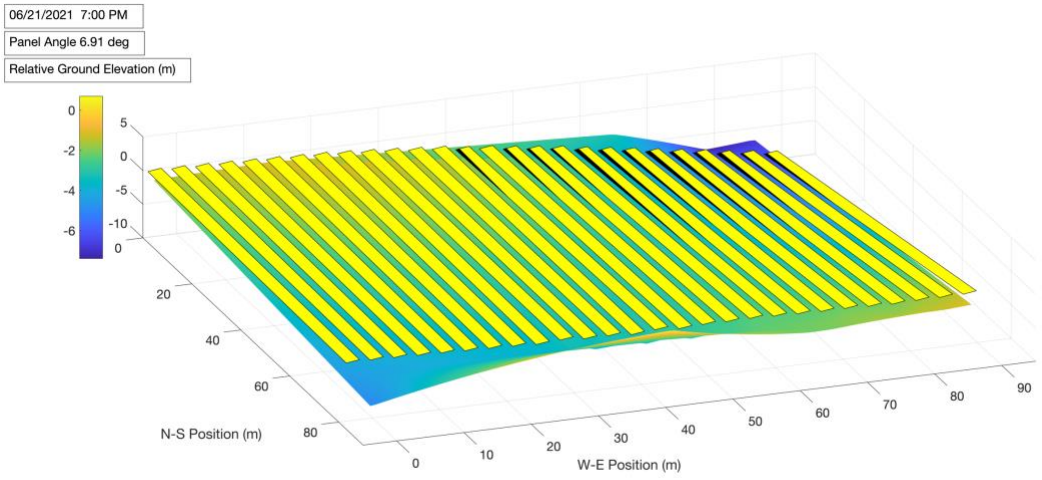

Figure 3.8 Shading for Z1 on June 21st at 7 pm. All 26 rows of Z1 are shown as well as the last row of the neighboring zone. Yellow corresponds to panels that are seeing sun where the black is the shading pattern. The gradient shape represents the uneven ground. Several rows on the east side are substantially shaded due to the decrease in ground elevation.

Figure 3.8 shows the entire zone Z1 and the shading patterns expected on June 21st at 7 pm. Since the east side of the field is downhill, there is substantial shading on 13 of the 26 rows. The shading shapes seen are consistent with those reported from measurements at the solar farm.

3.9 Power

Finally, the power output for the panels can be calculated. A power subroutine takes in the shading shape and size, cell temperature, and POA irradiance. This subroutine uses functions provided by PVLib and custom code developed by Andy Kim to accurately predict the power output for an entire row [12].

The power outputted by a solar panel is dependent on its I-V curve. This curve plots current against voltage and is used to find the maximum power point (MPP). I-V curves change consistently with temperature and irradiation, so a maximum power point tracking (MPPT) controller is used to create the I-V curve and to find the MPP throughout the day. To model this, PVLib has functions to find where the current and voltage multiply to give the greatest power output. This is considered to be the power outputted by the panel before shading is taken into account.

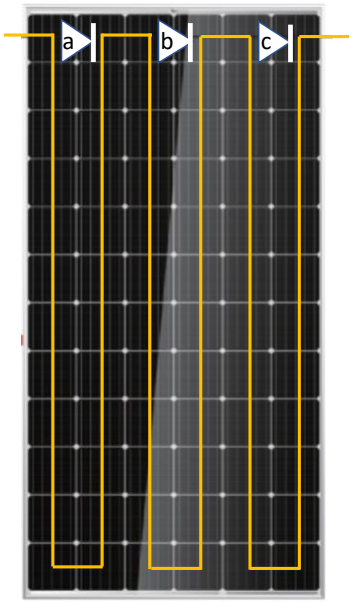

Figure 3.9 Solar panel schematic with diodes and substrings. If one substring loses power due to shading, the diode can bypass it.

Figure 3.9 shows how the panels at the solar farm for the zone being modeled are connected. There are three diodes that split the 72 cells into substrings of 24 cells connected in series. For these panels, it is assumed that once the bottom cell in a substring has 30% shading, the entire substring is unable to produce power since they are connected with the same current. If one substring is shut off, the diodes can be used to ignore that substring and allow for the rest of the substrings to remain on and producing power. Figure 3.10 shows the effect that shading has on the power for the substring and the panel. When the bottom cell is

minimally shaded, the power output decreases linearly until dropping instantly at 30% shading. The other two substrings can still produce power if they are not shaded. This shading model is used in conjunction with the MPP to find the actual power produced by the panels at any point in time.

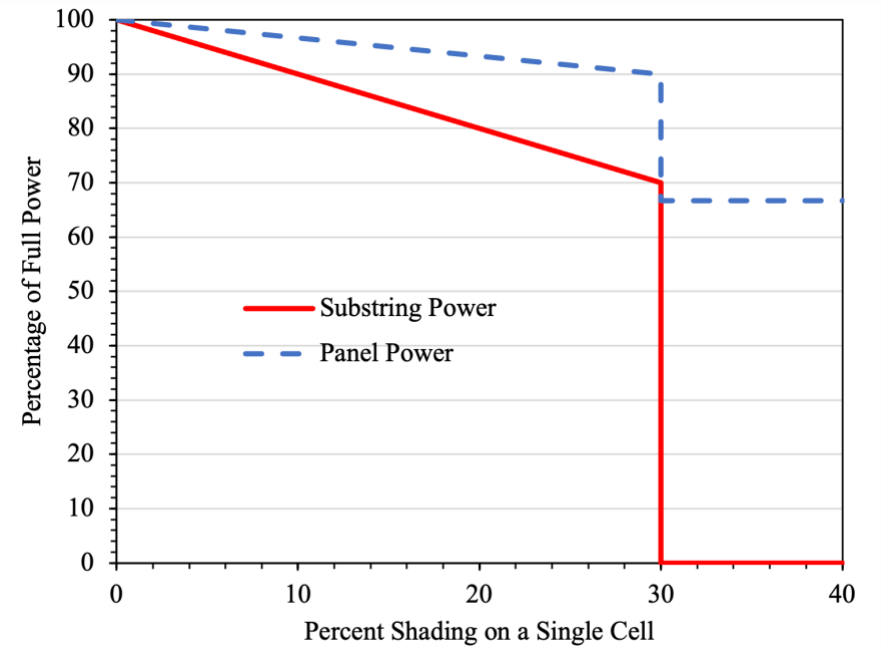

Figure 3.10 Percent of power versus percent shading on the bottom cell of the substring. As the shading begins to the cover the bottom cell, the power in the substring and panel begin to decrease linearly. At 30% shaded, the bottom cell fails to produce current, and the substring stops producing power. The other 2 substrings can continue to produce power in the panel.

Chapter 4

POINT IN TIME DATA MATCHING

Once the model was created, it was validated using actual data coming from the GPM at the Gold Tree Solar Farm. Shade lengths and heights, power output, cell temperature, and panel tilt angle were all collected and compared to the predicted values from the model.

4.1 Data Collection Techniques

The GPM was able to provide data on power output for each inverter and the expected panel tilt. Each inverter is connected to three rows, and for this validation, inverter 55 is analyzed. This inverter is connected to rows 541, 542, and 543, where row 540 was used to predict the shading on 541. Table 4.1 provides the coordinates for these rows in units of feet. Figure 4.1 shows inverter 55's location in the solar field and the corresponding rows. It also shows where inverter 52 is used as a basis for unshaded power.

Table 4.1 Torque tube coordinates for the three rows connected to inverter 55 and row 540 which shades the first row in the afternoon. All coordinates are in feet.

	Torque Tube North End			Torque Tube South End		
Row	x	y	z	x	y	z
540	23.57	176.10	-4.29	276.83	183.00	-2.54
541	25.07	187.28	-5.60	278.33	194.17	-2.31
542	26.55	198.30	-6.76	279.80	205.13	-2.08
543	28.02	209.33	-7.83	281.28	216.16	-1.71

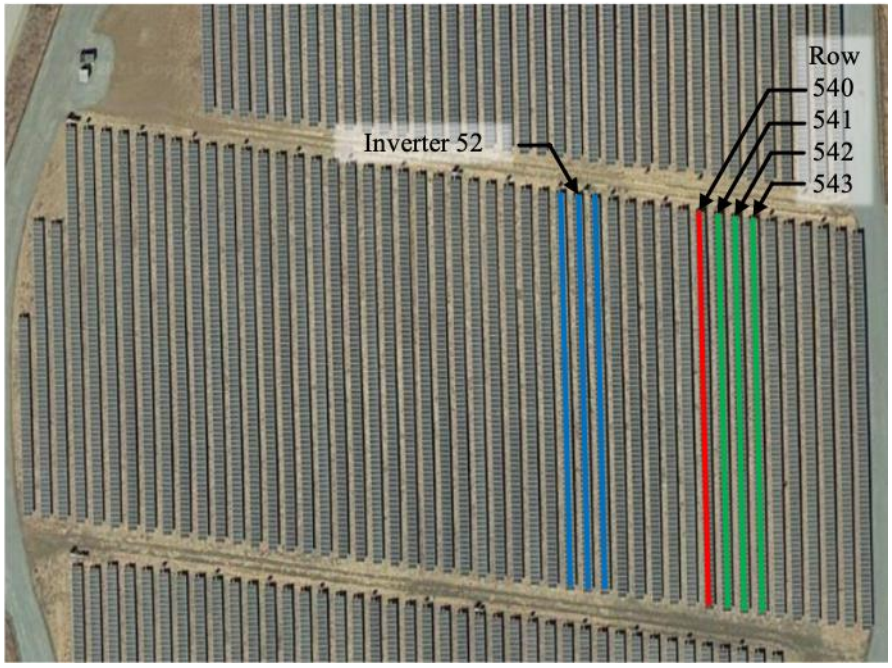

Figure 4.1 Inverter 55 and 52 locations at the Gold Tree Solar Farm. Inverter 55 is the inverter being analyzed and inverter 52 is used as an unshaded reference. Inverter 55 is connected to rows 541 through 543. Row 540 shades the first row of inverter 55 in the afternoon.

Inverter 52 was used to back-calculate the POA irradiance seen at the solar field. Since inverter 52 is unshaded, the power model could be used to determine the irradiance seen for this particular zone at any point in time if given the cell temperature. The temperature of the cell was collected using a handheld infrared thermometer pointed at the back of the panels. Since there are many panels in a row, an average was taken across the three rows that connect to inverter 55. After gathering the cell temperature and POA irradiance, the model could predict the shape and size of shading and therefore the power output for each row.

To validate the shade shapes and sizes, masking tape was put on the panels where the shading started and stopped immediately after the panels moved. It was important to collect data immediately since the rows move every five minutes on average, and the shading size changes quickly in the late afternoon as the sun drops. A tape measure was used to find the length and height of the shade on each row connecting to inverter 55. The shape of the shading on these rows was always a triangle with no offset along the panels. The angles of rows 540, 541, 542, and 543 were also taken using an Empire Level Dial Protractor to predict the shading more accurately.

4.2 October 16th, 2020 Data Matching

Data was taken on October 16th, 2020 at the Gold Tree Solar Farm. At four different times, the cell temperature, power output, tracker angle, actual panel angles, and shade sizes were found. Table 4.2 shows the POA irradiance, tracker angle, and cell temperature at each time. The POA irradiance was back-calculated using the GPM outputted power for inverter 52 at each of the times and the cell temperature. The tracker angle was given by the GPM as the panel tilt angle expected. Finally, the cell temperature was found as described in Section 4.1 using an infrared thermometer.

Table 4.2 POA irradiance, tracking angle, and cell temperature data for October 16th, 2020. POA irradiance was found using the power from inverter 52. The tracker angle is the angle outputted by the GPM for the set panel tilt. The cell temperature was measured using an infrared thermometer on the back of the panels.

Time	POA Irradiance (W/m^2)	Tracker Angle (degrees)	Cell Temperature (°F)
3:45 PM	520	22.70	103
3:50 PM	510	21.12	102
4:10 PM	454	16.18	102
4:37 PM	367	13.00	90

4.2.1 Panel Tilt Angle

Table 4.3 shows how the tracker angles compare to the actual panel angels at the solar farm. For each of the four times that data was collected at, the actual angles were two to three degrees larger than the modeled angles. The angles were reported to half a degree but varied by up to two and a half degrees between rows for the entire zone. This variance is not predicted by the model because it is due to outside factors. The effects of the variance in panel tilt are investigated in Section 6.4. The modeled panel angle and the actual panel angle are often off by up to 2 degrees which makes the shading difficult to predict for a single point in time. Because of this, the shade sizing is modeled using the actual panel angles instead of the modeled angles.

Table 4.3 Modeled panel angle vs actual panel angle at four different times on October 21st, 2020, for each row connected to inverter 55. The actual panel angle is larger than the modeled panel angle and has fluctuations that do not occur in the model.

Time	Row	Modeled Panel Angle (degrees)	Actual Panel Angle (degrees)	Angle Difference
3:45 pm	541	23.38	27.0	-3.62
	542	23.38	26.5	-3.12
	543	23.38	26.5	-3.12
3:50 pm	541	21.78	24.5	-2.72
	542	21.78	24.5	-2.72
	543	21.78	24.0	-2.22
4:10 pm	541	16.81	20.0	-3.19
	542	16.81	20.0	-3.19
	543	16.81	19.5	-2.69
4:37 pm	541	12.03	15.5	-3.47
	542	12.03	15.0	-2.97
	543	12.03	15.5	-3.47

4.2.2 Shading Size

Figure 4.2 shows the shading seen on row 541 in the afternoon. The shading shape is a triangle, and this triangle grows in height and length as time passes. When collecting data, the height and length were marked with blue tape and measured later due to the speed at which the shade grows, especially in the late afternoon. Also of note, the panel shown is no longer producing power since the shade is almost entirely covering the first cell of all six columns.

Figure 4.2 Actual shading seen at the Gold Tree Solar Farm. The shade shape is a triangle extending across the row. As time passes, this triangle grows in area.

Table 4.4 compares the predicted and actual shade height and length for each of the rows at the four times analyzed. The actual length of the shade is less than the modeled shade by anywhere from 5 to 60 percent. The actual height of the shade is also less than the modeled shade but only by 3 to 32 percent. The model appears to overestimate the amount of shading at any given time. The percent difference fluctuates from row to row and between times.

The model may be unable to accurately calculate the shading because of the various sensitivities that are discussed in Chapter 6. Due to the number of variables and their high variances, the model has difficulty in predicting the shade size at a single point in time. To correctly calculate the size of the shading, precise measurements of panel tilt, torque tube coordinates, and solar position must be taken and compared to the corresponding shade measurements given at a specific point in time at the field.

Table 4.4 Modeled shade vs actual shade at four different times on October 21st, 2020 for each row connected to inverter 55. The modeled shade is found using the measured angles of the panels and is consistently an overestimate of the actual shade.

		Modeled Shade		Actual Shade		Percent Difference	
Time	Row	Length (ft)	Height (in)	Length (ft)	Height (in)	Length	Height
3:45 pm	541	89.6	6.09	77.5	4.63	16%	32%
	542	91.5	5.55	70.6	4.88	30%	14%
	543	73.8	4.83	64.6	5.13	14%	6%
3:50 pm	541	92.1	6.60	80.5	5.88	14%	12%
	542	93.6	5.97	80.2	6.13	17%	3%
	543	74.1	5.11	70.3	6.25	5%	18%
4:10 pm	541	137.3	11.71	99.0	10.25	39%	14%
	542	134.5	10.26	100.6	10.00	34%	3%
	543	111.9	9.21	93.4	10.13	20%	9%
4:37 pm	541	183.2	20.16	114.4	18.25	60%	10%
	542	172.9	17.32	118.6	16.75	46%	3%
	543	153.4	16.17	116.5	17.13	32%	6%

4.2.3 Inverter 55 Power Output

Since the shading prediction is inaccurate, the power outputted to inverter 55 is expected to be inaccurate at a point in time. Table 4.5 shows the modeled power and the actual power to inverter 55 and how they compare. For the first three times, the actual power is about 30% more than the modeled power. For the last time, the actual power is 59% more than the modeled power. This could be attributed to the increased sensitivity as the sun continues to set. The smaller solar elevation angles and flatter panel tilt angles create a more sensitive system that is harder to model accurately. If the panels were modeled with more precise measurements, the power outputted would likely match better to actual data.

Table 4.5 Modeled power vs actual power at four different times on October 21st, 2020 for inverter 55. The actual power outputted is consistently higher than the modeled power and is around 30% higher for three out of four times.

Time	Modeled Power (kW)	Actual Power (kW)	Percent Difference
3:45 pm	22.2	31.3	-29%
3:50 pm	20.81	29.1	-29%
4:10 pm	15.87	22.8	-30%
4:37 pm	7.03	17.2	-59%

This analysis for a point in time shows the level of precision needed to effectively model shading and predict the power generation. However, it is not critical to match every point in time but instead to know the power output over a period of time. The optimization of the solar farm requires the power generation for an entire day to be accurate compared to actual data. Then, the backtracking settings can be adjusted to increase the power output and variable sensitivities will no longer affect the results as they are consistent for each day and will have less of an effect when integrated over time.

Chapter 5

DAY DATA MATCHING

Since modeling a point in time is difficult to validate, the power over an entire day was analyzed and compared to the outputted power by the GPM for inverter 55. By analyzing an entire day, many of the sensitives become less influential as time is integrated over. A relatively sunny day out of every month was compared and the two extremes are shown here for January and June. The comparisons were performed using all modeled parameters including ambient temperature, irradiance, and wind speed to predict the power output.

5.1 June 18th, 2020

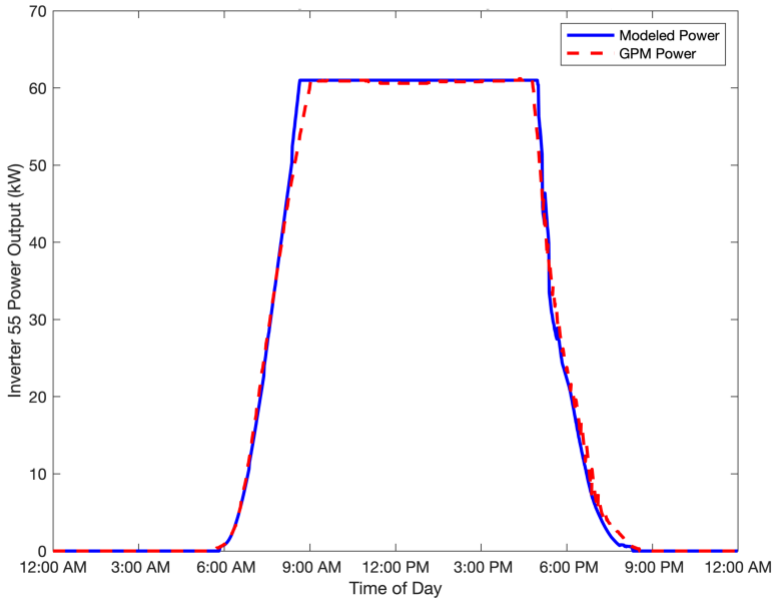

Figure 5.1 Modeled vs actual power out of inverter 55 for June 18th, 2020. The modeled power and actual power closely match including in the morning and afternoons when backtracking is occurring. The power level caps at around 60 kW due to the inverter's continuous power rating.

The modeled power and actual power closely match in shape and value, as seen in Figure 5.1 for June 18th, 2020. This offers the conclusion that the model is effective at predicting the power for a clear sunny day. The small amounts of error are likely due to imperfect predictions of cell temperature and POA irradiance, or environmental effects such as humidity and clouds. Both the actual and modeled power are capped at about 60 kW due to the limitations of the inverter. Inverters have the highest efficiencies near their

continuous maximum limit and since the inverters see less than 60 kW in the winter months, the inverters are sized to have the highest efficiency over the course of the year. When the power is not a maximum, the model is still accurately predicting the power output. Thus, the model is effective in the backtracking region.

5.2 January 16th, 2021

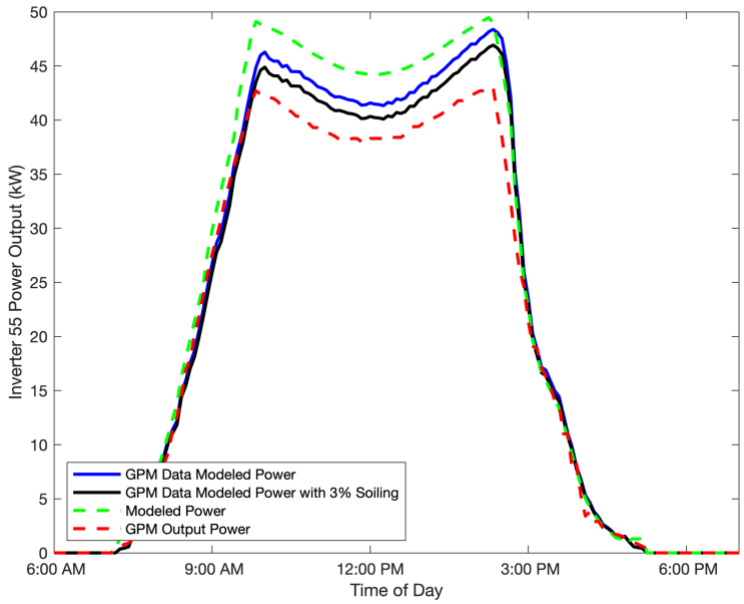

Figure 5.2 Modeled vs actual power out of inverter 55 for January 16th, 2021. The highest line is the pure model prediction for power. The next two highest lines are the power predicted using GPM data for POA irradiance and ambient temperature where the lower line also includes a 3% soiling factor. The bottom line is the actual power outputted by the inverter. All lines are relatively effective at predicting the backtracking region but are higher during the middle of the day during peak power generation.

The power predicted using the pure model, the power predicted using the ambient temperature and POA irradiance given by the GPM, the power using the ambient temperature and POA irradiance with 3% soiling, and the actual GPM outputted power by the inverter are shown in Figure 5.2. The power predicted using the pure model with no outside data is the highest power on the graph. This model still predicts the ramps where backtracking occurs relatively well but overpredicts the power during the middle of the day. This is partially due to the ambient temperature being much lower than the actual ambient temperature. Using the NREL weather predictions for a typical month means the actual temperature is much higher since the winter months have many cloudy and rainy days. The GPM data power curve on the graph shows the power output with more certainty since it uses actual data for ambient temperature and POA irradiance. The POA

irradiance is measured off a different zone, however, Figure 5.3 shows how similar the modeled and actual POA are especially in the backtracking regions. To improve the power prediction even further, a 3% soiling factor was placed on the curve to simulate the dust and pollen that often covers the panels. All of the power curves are effective at predicting the power during the backtracking region but overpredict output throughout the middle of the day. This shows the importance of cell temperature on the power output and the need for an accurate cell temperature model to precisely predict power output for a given day. The overprediction might also be a result of the degradation of the cells but further experimentation would be needed to verify.

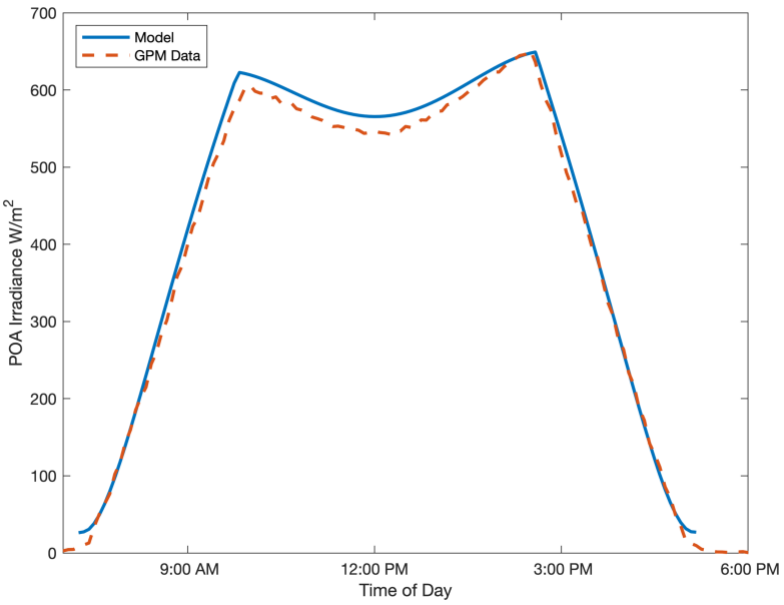

Figure 5.3 Modeled vs actual POA irradiance for January 16th, 2021. The actual POA irradiance is measured from a different zone but the overall shape and size of the two curves are very close to each other.

Since the power model consistently overpredicts output in the middle of the day, the optimization of the solar farm will not be affected. The accurate modeling of the backtracking region is the only critical part of maximizing the power and reducing the shading. Therefore, the model is validated to be used for optimization but requires further refinement to accurately predict power for any day.

Chapter 6

SENSITIVITY

6.1 Solar Position Models

To determine the precise position of the sun in the sky, several different models were used. Since shade height is much more sensitive to sun elevation than sun azimuth, elevation angle was the variable of concern. The models that were investigated were from Seinfeld and Pandis [13], Szolokay [14], PVLib, and two websites: SunCalc.org [15] and Keisan Online Calculators [16]. Table 6.1 shows how the height of shade changes with elevation angle for row 541 of zone Z1. The models all had the same latitude, longitude, and altitude inputs for October 16th, 2020, at 3:45 pm. The angles were then plotted as vertical lines. The actual shade height was 4.625 inches which is lower than any of the model's predictions. This could be due to incorrect coordinates for row 541 or the sensitivity of shade to time which is discussed in Section 6.3.

Table 6.1 Varying sun elevation models and their effect on shading for October 16th, 2020 at 3:45 pm. The PVLib Equation was chosen to model the location of the sun in the sky. It matched the SunCalc.org online calculator and is within less than half a degree of the other models except the Seinfeld model. The height of shade for row 541 is also shown and how it decreases with increasing elevation angle.

	Seinfeld & Pandis	SunCalc.org	PVLib Equation	Szokolay Equation	Keisan Online Calculator
Elevation Angle (deg)	28.11	28.94	28.94	29.05	29.23
Height of Shade (in)	7.73	6.15	6.15	5.94	5.60

The Seinfeld and Pandis equation that is also cited on Wikipedia presented the greatest discrepancy in actual shade height at 3:45pm when compared to other models. All four of the other models investigated were within .3 degrees of each other which corresponds to a change in height of .5 inches. Over the course of a full day or a full month, a half an inch change in height will not change the energy output enough to consider a more precise model. Therefore, the PVLib model was used as it was previously created for MATLAB and presented adequate accuracy to predict power.

6.2 Coordinate Sensitivity

The amount of shading is affected by many variables including the location of the torque tubes, the panel tilt angle, and the time of day. The following sensitivity analysis was performed on a perfectly north-south aligned solar field at a time of 4:37 pm on October 16th, 2020. At this time and date, the shading is large and many of the panels have lost power. This analysis focuses on row 541 and how row 540 shades it. These rows are in zone Z1 and row 541 connects to inverter 55. The following plots and discussion do not accurately represent real-world data but instead, investigate a single variable's effect on the extent of shading.

When changing the x-coordinate of the north end of the torque tube, the height of the shade increases, and the length of the shade decreases as seen in Figure 6.1. The x-coordinate corresponds to the north direction. Therefore, as the coordinate of row 541 moves further north by 1 inch the shading height increases by .011 inches and the length decreases by .627 inches. Similar sensitivities are seen when changing the x-coordinate of row 540.

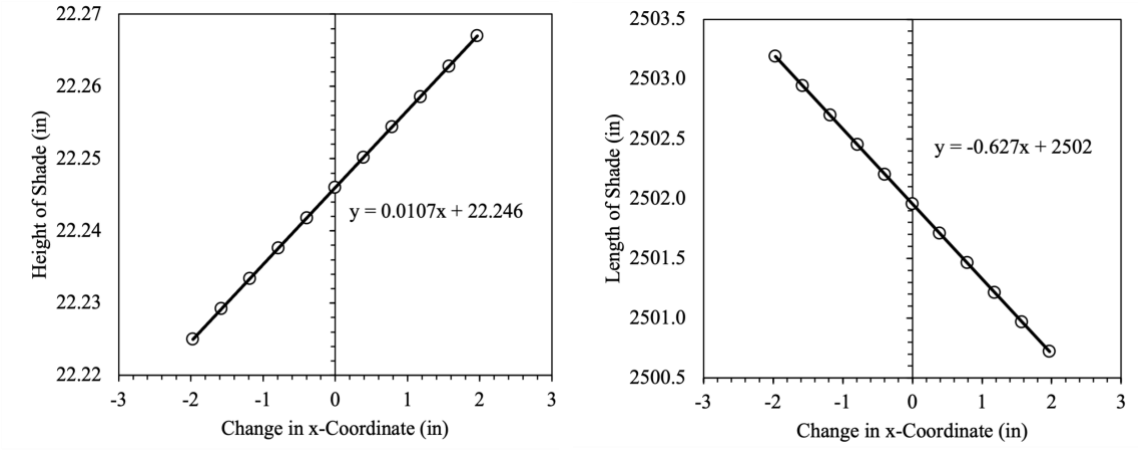

Figure 6.1 Change in x-coordinate of row 541 and its effect on the height and length of the shade. A one-inch change in the x-coordinate causes a .01-inch increase in height and a .63-inch decrease in length.

A similar analysis can be made on the y-coordinate for the north end of the torque tube. A change in shading occurs with varying y-coordinates, as seen in Figure 6.2. Increasing the y-coordinate by an inch decreases the height of the shade by .578 inches and the length by 11.045 inches. Since the panels are effectively moving farther apart, the shade should decrease when the y-coordinate decreases. Moving row 540 instead of 541 yields similar sensitivities.

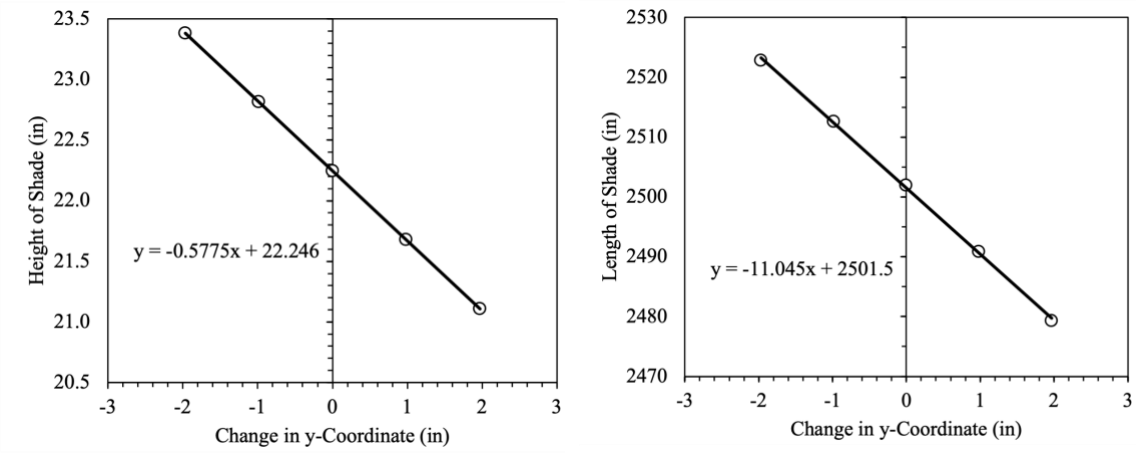

Figure 6.2 Change in y-coordinate of row 541 and its effect on the height and length of the shade. A one-inch change in the y-coordinate causes a .58-inch decrease in height and a 11.0-inch decrease in length.

Finally, the z-coordinate's effect on shading can be seen in Figure 6.3. The z-coordinate corresponds to the height of the torque tube off the ground relative to the first row. When the z-coordinate for the north end of the torque tube increases by an inch, the height of shading decreases by 1.464 inches and the length decreases by 28.208 inches. When changing row 540, similar sensitivities are seen, but the slope of the trendline is in the opposite direction. This is because the row that is causing the shading is increasing in height instead of the row being raised.

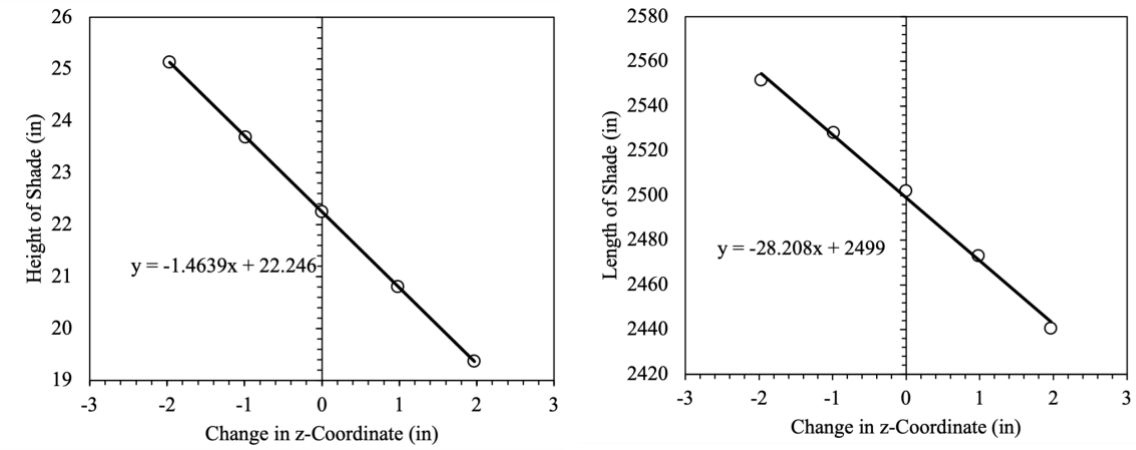

Figure 6.3 Change in z-coordinate of row 541 and its effect on the height and length of the shade. A one-inch change in the z-coordinate causes a 1.46-inch decrease in height and a 28.21-inch decrease in length.

When modeling a solar field, it is important to get accurate coordinates to be able to predict shading and thus power output. The most sensitive dimension is the height of the torque tube followed by the east-west coordinate that corresponds to the spacing between rows. These sensitivities can change with respect to time as the sun gets lower in the sky and are most important when there is enough shading to reduce the power significantly.

6.3 Time Sensitivity

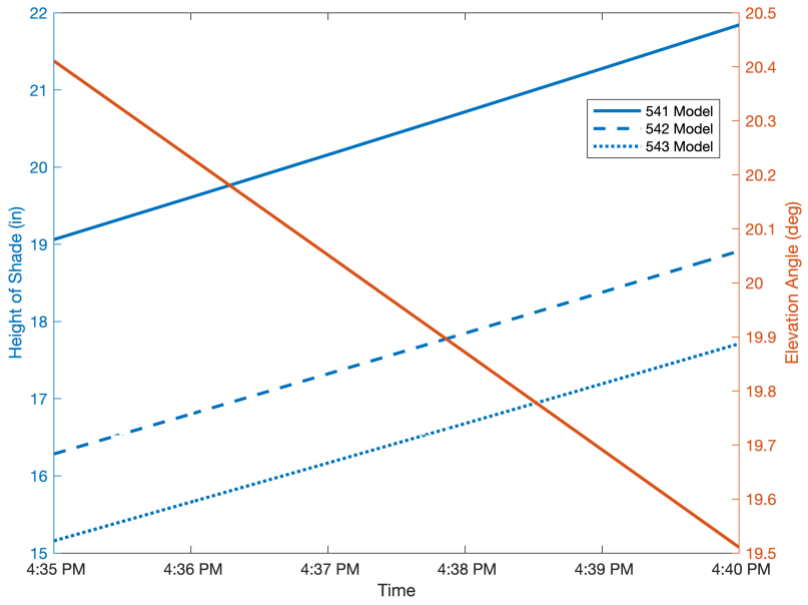

Figure 6.4 Height of shade and elevation angle change over five minutes for October 16th, 2020. Over five minutes, the height of the shading on rows 541, 542, and 543 increases by more than 2.5 inches. The sun elevation decreasing by almost a degree causes this increase in shading.

While taking measurements on-site, the shading was observed to increase rapidly when the panels stayed stationary for roughly five minutes. Utilizing the model, the shade height increased by 2.78 inches for row 541, 2.63 inches for row 542, and 2.55 inches for row 543 over a five-minute interval which can be seen in Figure 6.4. The .9 degree change in elevation of the sun causes this change in the height of shading. This model is based on the actual coordinates of the as-built torque tubes and the panel tilt angles at 4:37pm on October 16th, 2020. The sensitivity to time is not linear for an entire day. It is instead dependent on how close the sun elevation angle is to the horizon. When the sun is high in the sky, any shading that occurs grows

slowly, whereas closer to sunrise or sunset, the shading size can grow very quickly. Since the height of shade changes rapidly for the point in time data analysis, shade measurements were taken quickly to obtain the most accurate data.

6.4 Panel Tilt Sensitivity

Along with time and location, the tilt of the row also affects the height of shading significantly. For this sensitivity analysis, rows 540, 541 and 542 were modeled on October 16th, 2020 at 4:37 pm using the as-built coordinates. Rows 540 and 542 were held at a constant 14 degrees, while Row 541 was changed from 13 to 15 degrees. As seen in Figure 6.5, the shade height on Row 541 increased by .615 inches for every degree and the shade height on Row 542 increased by .842 inches per degree. The angles of the panels were typically ± 2 degrees off the expected angle when measured in the field. This could be attributed to the lack of tight tolerances on the cams controlling the tilt angle. The rows can also slip relative to the drivetrain when strong winds occur and may not be properly calibrated when reattached. No matter the cause, large fluctuations in panel tilt have a dramatic effect on the shading. This effect is not perfectly linear and changes with time. In order to obtain accurate shading measurements, the angle of each panel needs to be known.

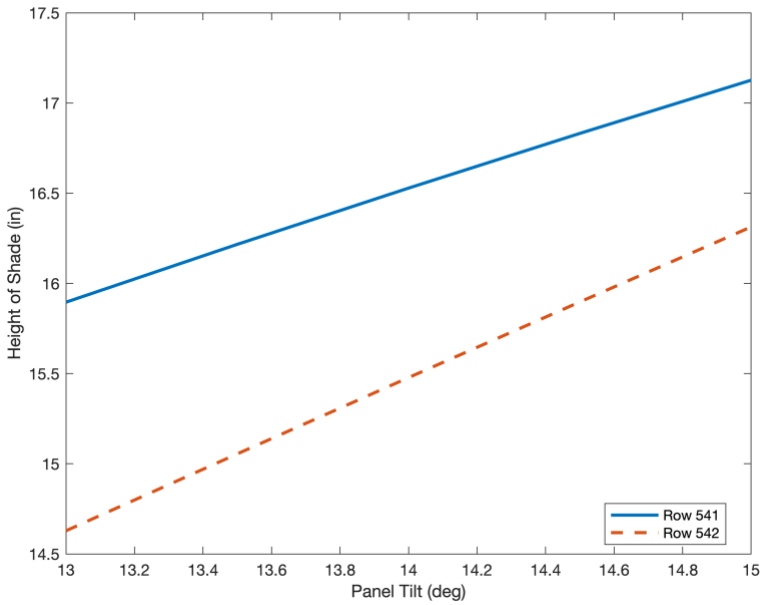

Figure 6.5 Height of shade for change in panel tilt of row 541. Row 541's shade increases by .615 inches per degree. Row 542 shading is also shown and increases by .842 inches per degree.

Chapter 7

OPTIMIZATION OF POWER OUTPUT

7.1 Predicted Baselines

Table 7.1 Unshaded and shaded energy predictions for each month assuming it is always sunny. Both predictions use a torque tube spacing of 11 ft, but the unshaded prediction assumes no interrow shading. This provides a maximum amount of energy that could theoretically be produced if the field was perfectly flat. The shaded energy predictions account for the shading and are then compared to the theoretical maximum as a percentage.

Month	Unshaded Energy (kWh)	Shaded Energy (kWh)	Percent of Maximum
January	94,206	80,709	85.7%
February	109,723	94,713	86.3%
March	145,930	126,750	86.9%
April	158,540	137,612	86.8%
May	177,453	154,074	86.8%
June	176,669	153,989	87.2%
July	180,238	156,603	86.9%
August	169,734	146,929	86.6%
September	149,456	129,202	86.4%
October	125,005	108,518	86.8%
November	97,937	83,933	85.7%
December	86,052	73,412	85.3%
Year	1,670,945	1,446,442	86.6%

After validating the model, the predicted energy produced was determined using the nominal torque tube spacing of 11 feet. First, the model was used to predict the energy with backtracking but no shading. This provides a theoretical maximum of how much energy could be produced for each month if every day was sunny and there was no shading at the field. Next, the model predicted the monthly energy produced with shading. Again, the model assumes every day is sunny so predicted energy values for each month are much higher than actual data. Table 7.1 summarizes the results obtained for each month, as well as how much the shaded energy is as a percentage of the unshaded theoretical maximum. The yearly total is also included. If the 11 feet torque tube spacing is used, the solar farm is only operating at about 85 to 87 percent of the

theoretical maximum due to the shading occurring. By changing the torque tube spacing in the backtracking algorithm, the amount of shading can be decreased and therefore the energy output increased.

7.2 Optimization Methods

To maximize the energy output at the solar farm, the morning and afternoon modified torque tube spacings had to be optimized. Initially, MATLAB's internal optimization toolbox was used to perform an optimization. Due to the sensitivity and the large number of variables, the built-in optimization algorithms were ineffective at maximizing the energy. Thus, manual optimization using MATLAB was required as shown in Appendix D.

First, the west torque tube spacing (for the afternoon) was incrementally varied over more than two and a half feet. The monthly energy was then predicted and a rough estimate of the optimized tube spacing was found. Figure 7.1 shows how the monthly energy varied as well as the maximum occurring somewhere near 9 feet.

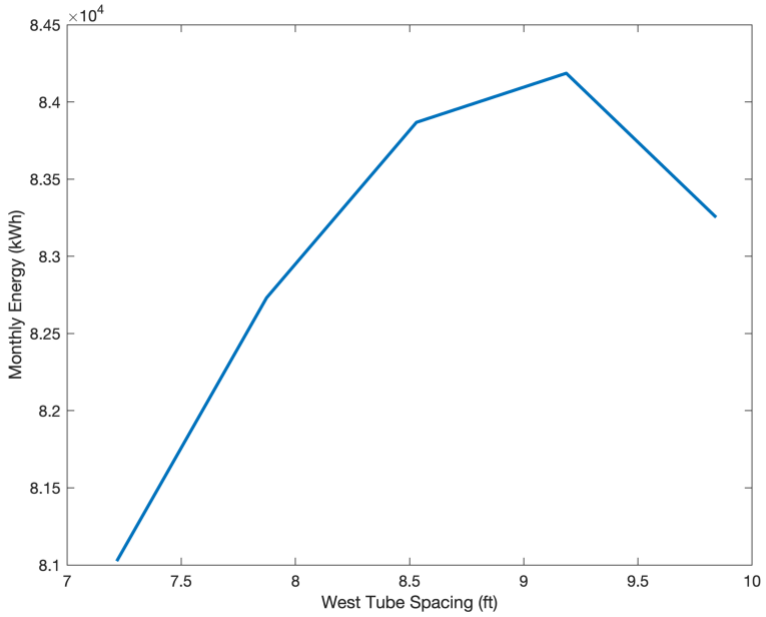

Figure 7.1 Monthly energy vs west torque tube spacing for January. As the torque tube spacing was varied, the monthly energy curve was created. The maximum monthly energy occurred just above 9 feet.

After having a rough estimate for where the maximum energy occurred for every month, a smaller span of torque tube spacings was analyzed at a smaller increment of .05 feet or approximately .6 inches. By

refining the monthly energy curve, a more precise prediction and optimization can be made. Figure 7.2 shows the new zoomed-in monthly energy curve and provides the maximum energy point at 9.07 ft for January.

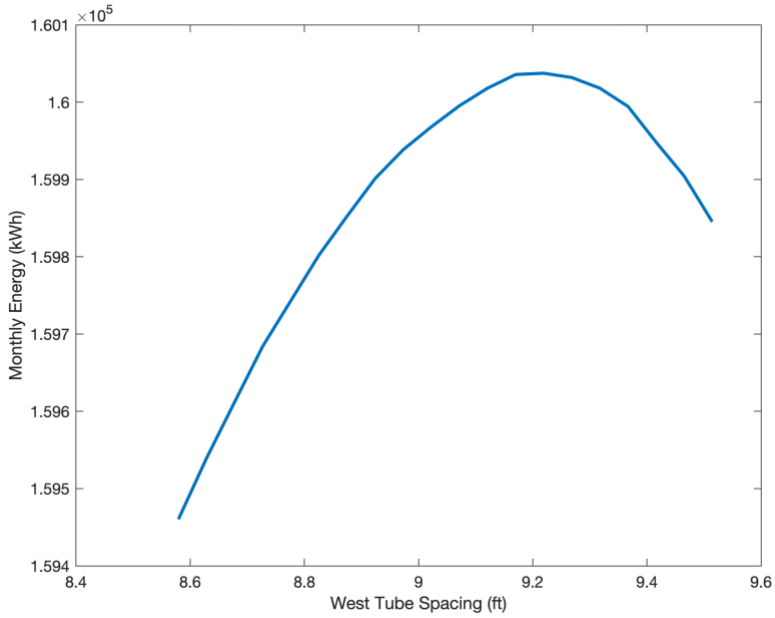

Figure 7.2 Refined monthly energy vs west torque tube spacing for January. The maximum monthly energy occurs at a west torque tube spacing of 9.07 feet.

The shows the refined optimization curves every month as well as the nominal monthly energy when the backtracking is set to 11 feet can be seen in Figure 7.3. All the curves are normalized to the theoretical maximum when there is no shading at all for a backtracking setting of 11 feet. The curves are similar in shape, and the maximum points are labeled with their corresponding optimum torque tube spacing. The summer months are closer to the theoretical maximum for both the optimization curve and for the nominal monthly energy. With just the west torque tube spacing optimized, the monthly energy is increased to around 90 percent of the theoretical maximum.

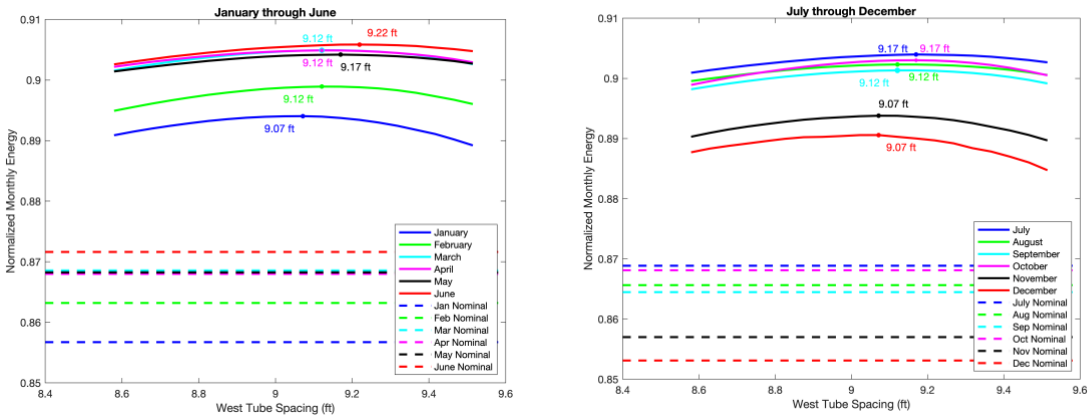

Figure 7.3 Optimization curves and nominal energies for each month. All the curves are normalized to the theoretical maximum energy. Each curve shows the shape of the optimization and where the maximum point is. All curves are based only on the west torque tube spacing optimization.

After the afternoon optimization process was repeated for every month, it was then repeated for the east torque tube spacing (for the morning). Table 7.2 summarizes the optimized west and east torque tube spacings for each month. Some values repeat because the increment is not large enough to obtain distinct values for each month. Using a smaller increment could produce even more optimized values, but the monthly energies would only change by a few kilowatt hours. It also can be observed that the west torque tube spacings increase in the summer months while the east torque tube spacings increase in the winter months. This discrepancy is sensible especially since the rows themselves are about 1.5 degrees off true north. After finding all the optimized torque tube spacings, the maximum energy for each month could be predicted.

Table 7.2 Optimized west and east torque tube spacings for each month. The west torque tube spacings are large in the summer while the east torque tube spacings are larger in the winter.

Month	West Tube Spacing (ft)	East Tube Spacing (ft)
January	9.07	10.14
February	9.12	10.14
March	9.12	9.71
April	9.12	9.60
May	9.17	9.55
June	9.22	9.50
July	9.17	9.50
August	9.12	9.55
September	9.12	9.65
October	9.17	9.79
November	9.07	9.84
December	9.07	9.79

7.3 Optimized Energy

Table 7.3 Optimized energy and its comparisons to the theoretical maximum and the nominal monthly energy assuming every day is sunny. The optimized energy is typically between 91 to 95% of the theoretical max for each month and about a 6 to 9% increase from the energy if the torque tube spacing was set to 11 feet.

Month	Optimized Energy (kWh)	Percent of Maximum	Energy Increase (kWh)	Percent Increase
January	86,261	91.6%	5,552	6.88%
February	101,319	92.3%	6,606	6.98%
March	136,564	93.6%	9,814	7.74%
April	149,608	94.4%	11,996	8.72%
May	168,006	94.7%	13,932	9.04%
June	167,466	94.8%	13,478	8.75%
July	170,626	94.7%	14,022	8.95%
August	160,112	94.3%	13,183	8.97%
September	139,945	93.6%	10,744	8.32%
October	116,091	92.9%	7,573	6.98%
November	89,717	91.6%	5,784	6.89%
December	78,423	91.1%	5,011	6.83%
Year	1,564,138	93.6%	117,695	8.14%

Each month was analyzed using the optimized torque tube spacings to predict the energy using the code. REC Solar requested a monthly basis as the ideal period to change backtracking settings. Different periods of time could be used to optimize the solar farm further but are unlikely to produce a meaningful change in energy. Table 7.3 shows the optimized energy as well as the comparisons to the theoretical maximum and nominal energy, as discussed in Section 7.1, for each month and the entire year. The optimized energy is within 91 to 95 percent of the theoretical maximum energy for each month and is 93.6 percent for the year. For winter months, the energy increase is seen to be around 5,000 kilowatt hours, whereas, in the summer it can be up to 14,000 kilowatt hours more than the nominal monthly energy where backtracking is set to 11 feet and shading is accounted for. As a percentage, the monthly energy is 6 to 9 percent more than the nominal and 8.14% more than the nominal energy for the year.

Comparing the nominal, optimized, and theoretical maximum energies, as seen in Figure 7.4, the optimized energy is a large increase from the nominal shaded energy. However, the optimized energy is still below the maximum theoretical energy for each month. This shows that the shading still has an impact and is not completely eliminated.

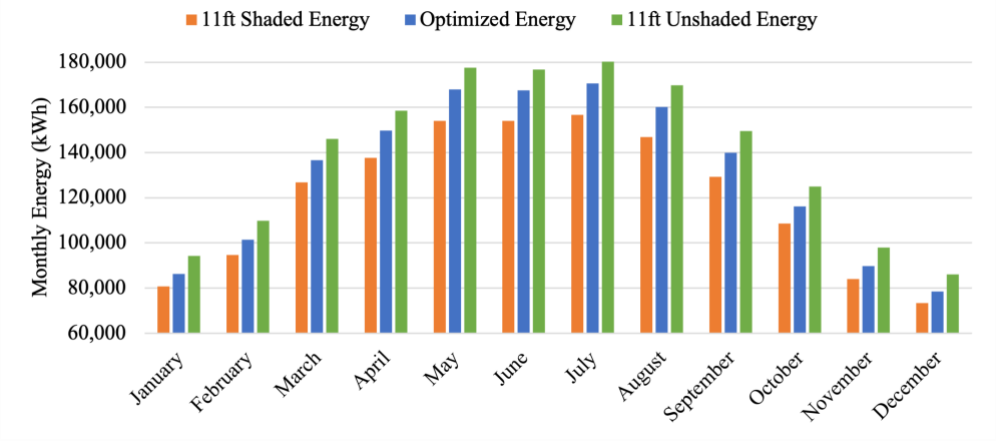

Figure 7.4 Nominal shaded energy, optimized energy, and theoretical maximum energies for each month. The optimized energy is approximately halfway between the nominal and maximum energies.

The percentage of zone Z1 that is predicted to be shaded for December 21st and June 21st, 2021 can be seen in Figure 7.5. When the torque tube spacing is higher, there is less backtracking and thus more shading. However, backtracking sooner means there is less POA irradiance and therefore less energy. The optimum backtracking settings are also shown and its effects on the percent shading. As can be seen, the optimum setting is not the minimum amount of shading. Additionally, the backtracking setting changes in the morning and afternoon which cause alterations in the percentage shaded changes as well.

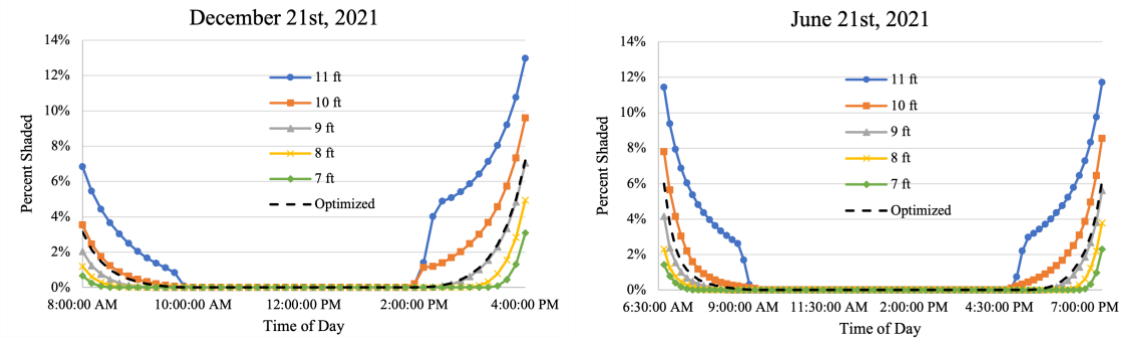

Figure 7.5 Percent area shaded on panels for December 21st and June 21st, 2021 for different modified torque tube spacings. The higher the modified torque tube spacing, the more shading there is throughout the day. The optimized value is not the minimum amount of shading but instead a balance between shading and POA irradiance.

7.4 Splitting Zone Z1 and Y4

To further optimize the solar farm, the adjacent zone, Y4, was analyzed. This specific zone only has 20 rows connected to a motor. Moving six rows from zone Z1 to Y4 could allow for an increase in production since these rows are on similar topography to zone Y4. Both January and June were analyzed as a representation of the total year. The optimization routine was run for both scenarios and both months. The energy increased but only by a small percentage as seen in Table 7.4. For January, the energy increased by .72 percent and for June, it increased by .30 percent. It is likely not worth switching the rows from Y4 to Z1 for such a small increase in monthly energy.

Table 7.4 Optimized energy s for splitting Z1 and Y4. The original and new configuration of switching 6 rows from Z1 to Y4 are shown as well as the energy and percent increase.

Month	Original Energy (kWh)	New Configuration Energy (kWh)	Energy Increase (kWh)	Percent Increase
January	156,908	158,004	1,096	.72%
June	300,188	301,080	893	.30%

Chapter 8

CONCLUSION AND FUTURE WORK

8.1 Conclusion

This thesis analyzed the Gold Tree Solar Farm and optimized the energy output by adjusting the backtracking algorithms. First, the power output for a single inverter was modeled for a single point and time and over the course of the day. The model was inadequate in predicting the power output of the inverter at a single point in time, as it consistently underpredicted the power output and overpredicted the amount of shading. This was likely due to the number and sensitivity of variables utilized, such as solar position, torque tube location, panel tilt, and time. Since it is difficult to predict the power output at a singular point in time, the power output for the inverter was compared over an entire day to the actual power output. The model was able to predict the power output during the backtracking regions effectively but overpredicted power output in the middle of the day. Cell temperature, degradation, and soiling could all be contributors to the overestimation. Since the model overpredicted consistently, the optimization routine was not affected and could still be used to maximize the monthly energy by changing the modified tube spacing.

The optimization adjusted the west and east modified tube spacing to maximize the energy output in the morning and afternoon for zone Z1. After optimization, the yearly energy output increased by 117,695 kilowatt hours or 8.14 percent. The model assumed that every day was clear and sunny, so the energy increase is likely to be much lower when applied to the real world. Optimizing the energy output did not eliminate the shading but instead balanced the shading and POA irradiance to find the maximum energy possible. Each month was optimized and the modified torque tube spacings were changed according to the changing azimuth and elevation of the sun. The adjacent zone to Z1, Y4, was also optimized for January and June to determine if switching six rows from Z1 to Y4 could further increase the energy output. The energy for January increased by .72 percent and the energy for June increased by .30 percent. This slight increase in energy is less than optimizing the zones themselves.

This thesis proved that the Gold Tree Solar Farm is not producing as much energy as it could be. The backtracking settings on sloped fields are difficult to predict on uneven topography; but with precise modeling, the energy output can be predicted. For this case study, the monthly energies were increased by 6 to 9 percent.

8.2 Future Work

The next step is to optimize the entire solar field after obtaining the locations of all the torque tubes. By optimizing all 12 zones, the energy output of the solar field can be greatly increased. This will supply Cal Poly with more energy and allow for greater profits. Each zone can be mapped using a LIDAR system to obtain more accurate torque tube coordinates and decrease the amount of time spent mapping the field.

In the future, the model can be refined and built upon to produce more accurate predictions. Cell temperature models can consider how the rows affect the wind through the solar field, and how much wind is actually on the surface of the panel. These models can also be revised to calculate the increased cell temperature when shaded since the energy is now all converted to heat instead of heat and electrical energy. Having a more accurate cell temperature along with accounting for soiling and degradation will provide more accurate power predictions.

Further in the future, the model can be used to predict ideal row spacing and backtracking settings before constructing the solar field to optimize energy output on sloped fields. With the increased use of solar energy, more commercial solar fields are likely to be built on skewed topography. The model would be a powerful tool to increase profits for solar companies and energy distributors while also decreasing the amount of land a solar farm will take up.

REFERENCES

[1] X. Sun, L. Cherry, and M. Cox, “Foresight 20/20: Solar supply chain, systems and technology,” *Wood Mackenzie*. Verisk, February 5, 2020. [Online] Available: https://www.woodmac.com/our-expertise/focus/Power--Renewables/solar-systech-foresight-2020/ [Accessed: 12-May- 2021]

[2] B. Nascimento, D. Albuquerque, M. Lima, and P. Sousa “Backtracking Algorithm for Single-Axis Solar Trackers installed in a sloping field,” *Journal of Engineering Research and Application*, December 2015.

[3] D. Dolan, V. Prodanov, P. Salter, F. Cheein and J. Dolan, "Reducing Performance Loss Due to Backtracking Error Through Use of Half Cut Cell Modules," *2019 9th International Conference on Power and Energy Systems (ICPES)*, 2019, pp. 1-4, doi: 10.1109/ICPES47639.2019.9105393.

[4] “GPM Portal,” *Green Power Monitor*. [Online]. Available: https://web3.greenpowermonitor.com/application/#/dashboard/3387. [Accessed: 12-Aug-2021].

[5] PV Performance Modeling Collaborative, “pvl_ephemeris”, *Sandia National Laboratories*. [Online]. Available: https://pvpmc.sandia.gov/PVLIB_Matlab_Help/ [Accessed 14-December- 2020]

[6] PV Performance Modeling Collaborative, “pvl_clearsky_ineichen”, *Sandia National Laboratories*. [Online]. Available: https://pvpmc.sandia.gov/PVLIB_Matlab_Help/ [Accessed 12-August- 2020]

[7] M. Lave, W. Hayes, A. Pohl and C. W. Hansen, "Evaluation of Global Horizontal Irradiance to Plane-of-Array Irradiance Models at Locations Across the United States," *IEEE Journal of Photovoltaics*, vol. 5, no. 2, pp. 597-606, March 2015.

[8] PV Performance Modeling Collaborative, “pvl_clearsky_ineichen,” *Sandia National Laboratories*. [Online]. Available: https://pvpmc.sandia.gov/PVLIB_Matlab_Help/ [Accessed 4-January- 2021]

[9] PV Performance Modeling Collaborative, “pvl_extraradiation,” *Sandia National Laboratories*. [Online]. Available: https://pvpmc.sandia.gov/PVLIB_Matlab_Help/ [Accessed 4-January- 2021]

[10] M. Mattei, G. Notton, C. Cristofari, M. Muselli, and P. Poggi, “Calculation of the polycrystalline PV module temperature using a simple method of energy balance,” *Renewable Energy*, vol. 31, no. 4, pp. 553–567, 2006.

[11] C. Schwingshackl, M. Petitta, J. E. Wagner, G. Belluardo, D. Moser, M. Castelli, M. Zebisch, and A. Tetzlaff, "Wind Effect on PV Module Temperature: Analysis of Different Techniques for an Accurate Estimation," *Energy Procedia*, vol. 40, pp. 77–86, 2013.

[12] B. Kim, "Solar Energy Generation Forecasting and Power Output Optimization of Utility Scale Solar Field," thesis, 2020.

[13] J. H. Seinfeld and S. N. Pandis, *Atmospheric Chemistry and Physics: From Pollution to Climate Change*. New York, NY: John Wiley et Sons, 2016.

[14] S. V. Szokolay, *Solar Geometry*. Brisbane, Qld.: PLEA, Passive and Low Energy Architecture International in association with Dept. of Architecture, University of Queensland, 1996.

[15] "SunCalc sun position," *SunCalc*. [Online]. Available: https://www.suncalc.org/#/35.3192,-120.6903,14/2020.10.16/15:45/1/3. [Accessed: 02-Nov-2020].

[16] "Solar elevation angle (for a day) Calculator," *Keisan Online Calculator*. [Online]. Available: https://keisan.casio.com/exec/system/1224682277. [Accessed: 02-Nov-2020].

Appendix A: Trina Solar Cell Datasheet

Mono Multi Solutions

TALLMAX M PLUS

TSM-DE14A (II)

THE FRAMED 72-CELL MODULE (1500V)

72 CELL
MONOCRYSTALLINE MODULE

340-375W
POWER OUTPUT RANGE

19.3%
MAXIMUM EFFICIENCY

0/+5W
POSITIVE POWER TOLERANCE

Founded in 1997, Trina Solar is the world's leading comprehensive solutions provider for solar energy. We believe close cooperation with our partners is critical to success. Trina Solar now distributes its PV products to over 60 countries all over the world. Trina Solar is able to provide exceptional service to each customer in each market and supplement our innovative, reliable products with the backing of Trina Solar as a strong, bankable partner. We are committed to building strategic, mutually beneficial collaboration with installers, developers, distributors and other partners.

Comprehensive Product And System Certificates

IEC61215/IEC61730/UL1703/IEC61701/IEC62716
ISO 9001: Quality Management System
ISO 14001: Environmental Management System
ISO14064: Greenhouse Gas Emissions Verification
OHSAS 18001: Occupational Health and Safety Management System

Trinasolar

Ideal for large scale installations
- High power footprint reduces installation time & BOS costs
- Reduce BOS cost by connecting more modules in a string
- 1500 V UL/1500 V IEC certied

Excellent low light performance on cloudy days, mornings and evenings
- Advanced surface texturing
- Back surface field
- Selective emitter

Maximize Limited Space with high efficiency
- Up to 193 W/m² power density
- Low thermal coefficients for greater energy production at high operating temperatures

Highly reliable due to stringent quality control
- All modules have to pass electroluminescence (EL) inspection
- Over 30 in-house tests (UV, TC, HF, and many more)
- In-house testing goes well beyond certification requirements
- PID resistant

Certified to withstand challenging environmental conditions
- Module coating resistant to sand, acid, and alkali
- 2400 Pa wind load
- 5400 Pa snow load
- 35 mm hail stones at 97 km/h

LINEAR PERFORMANCE WARRANTY

10 Year Product Warranty · 25 Year Linear Power Warranty

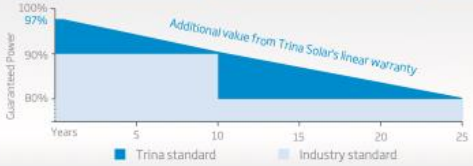

TALLMAX M PLUS

TSM-DE14A (II)

DIMENSIONS OF PV MODULE TSM-DE14A (II) (unit: mm)

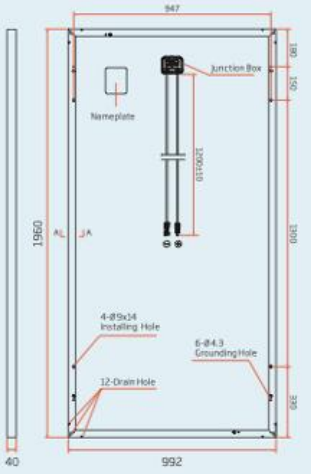

Back View

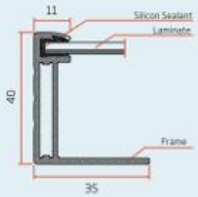

(A-A)

I-V CURVES OF PV MODULE (365W)

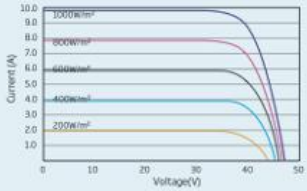

P-V CURVES OF PV MODULE (365W)

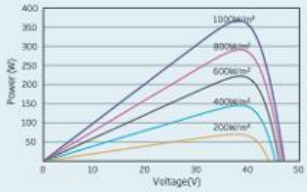

ELECTRICAL DATA @ STC	TSM-340	TSM-345	TSM-350	TSM-355	TSM-360	TSM-365	TSM-370	TSM-375
Peak Power Watts-P_{MAX} (Wp)*	340	345	350	355	360	365	370	375
Power Output Tolerance-P_{MAX} (W)	0/+5	0/+5	0/+5	0/+5	0/+5	0/+5	0/+5	0/+5
Maximum Power Voltage-V_{MPP} (V)	38.2	38.5	38.7	38.8	39.0	39.3	39.7	40.0
Maximum Power Current-I_{MPP} (A)	8.90	8.96	9.04	9.14	9.24	9.30	9.33	9.37
Open Circuit Voltage-V_{OC} (V)	46.2	46.7	47.0	47.4	47.7	48.0	48.3	48.5
Short Circuit Current-I_{SC} (A)	9.50	9.55	9.60	9.65	9.70	9.77	9.83	9.88
Module Efficiency η_m (%)	17.5	17.7	18.0	18.3	18.5	18.8	19.0	19.3

STC: Irradiance 1000 W/m², Cell Temperature 25 °C, Air Mass AM1.5
* Measuring tolerance: ±3%

ELECTRICAL DATA @ NOCT	TSM-340	TSM-345	TSM-350	TSM-355	TSM-360	TSM-365	TSM-370	TSM-375
Maximum Power-P_{MAX} (Wp)	253	257	261	264	268	272	276	279
Maximum Power Voltage-U_{MPP} (V)	35.4	35.7	35.9	36.0	36.2	36.4	36.8	37.1
Maximum Power Current-I_{MPP} (A)	7.15	7.20	7.26	7.34	7.42	7.47	7.50	7.53
Open Circuit Voltage-U_{OC} (V)	42.9	43.4	43.7	44.1	44.3	44.6	44.9	45.1
Short Circuit Current-I_{SC} (A)	7.67	7.71	7.75	7.79	7.83	7.89	7.94	7.98

NOCT: Irradiance at 800 W/m², Ambient Temperature 20 °C, Wind Speed 1 m/s.

MECHANICAL DATA

Solar Cells	Monocrystalline 156.75 × 156.75 mm
Cell Orientation	72 cells (6 x 12)
Module Dimensions	1960 × 992 × 40 mm
Weight	26.0 kg with 4.0 mm glass; 22.5 kg with 3.2 mm glass
Glass	4.0 mm for PERC Mono; 3.2 mm for Std Mono, high transparency, AR coated and heat tempered solar glass
Backsheet	White
Frame	Silver Anodized Aluminium Alloy
J-Box	IP 67 or IP 68 rated
Cables	Photovoltaic Technology Cable 4.0mm², 1200 mm
Connector	MC4 EVO2/UTX/TS4

TEMPERATURE RATINGS

Nominal Operating Cell Temperature (NOCT)	44°C (±2K)
Temperature Coefficient of P_{MAX}	- 0.39%/K
Temperature Coefficient of V_{OC}	- 0.29%/K
Temperature Coefficient of I_{SC}	0.05%/K

MAXIMUM RATINGS

Operational Temperature	-40 to +85°C
Maximum System Voltage	1000 V DC (IEC) 1000 V DC (UL)
Max Series Fuse Rating*	15 A (Power ≤ 350 W) 20 A (Power ≥ 355 W)
Mechanical Load	5400 Pa
Wind Load	2400 Pa

*DO NOT connect fuse in combiner box with two or more strings in parallel connection

WARRANTY

10 year Product Workmanship Warranty

25 year Linear Performance Warranty

(Please refer to product warranty for details)

PACKAGING CONFIGURATION

Modules per box:	27 pieces
Modules per 40' container:	648 pieces

TSM_EN_2017_B

Trinasolar

CAUTION: READ SAFETY AND INSTALLATION INSTRUCTIONS BEFORE USING THE PRODUCT.

www.trinasolar.com

Appendix B: Yaskawa Inverter Data Sheet

PVI 50TL-480 / PVI 60TL-480

3-PHASE TRANSFORMERLESS COMMERCIAL STRING INVERTERS

FEATURES

- Wirebox models with built-in SunSpec compliant transmitters for Module-Level Rapid Shutdown for simple, safe NEC compliance
- UL Listed as PV Rapid Shutdown Systems with Tigo Energy, APsmart and Northern Electric Power (NEP)
- Selectable Max AC Apparent Power 50kW/(50kVA or 55kVA) and 60kW/(60kW or 66kVA); 55kVA and 66kVA ratings allow Max Rated Real Power at +/- 0.91 PF
- Integrated UL-listed Arc-Fault protection
- 15 - 90° mounting angle allows low-profile rooftop installations
- 3 MPPTs with 5 fused inputs each for PV array flexibility
- Industry-leading DC/AC ratios of 1.8 (50TL) and 1.5 (60TL)
- Integrated AC and DC disconnects
- Remote firmware upgrades and diagnostics
- NEMA 4X outdoor rated enclosure, with proven performance
- UL1741SA certified to CA Rule 21, including SA14 FW and SA 15 VW

OPTIONS

- Shade cover
- DC fuse bypass
- Web-based monitoring

Yaskawa Solectria Solar's PVI 50TL-480 and PVI 60TL-480 are transformerless 3-phase inverters, ideal for rooftops, carports and ground-mount PV systems

The PVI 50TL-480 and PVI 60TL-480 come standard with AC and DC disconnects, three MPPTs, and a wiring box with 15 fuse positions.

For rooftop PV systems, three models provide PV Rapid Shutdown System (PVRSS) certification and include a wirebox with a built-in SunSpec-compliant powerline transmitter.

One wirebox model is Tigo Enhanced for rapid shutdown; other wirebox models are compatible with the APsmart and Northern Electric Power (NEP) rapid shutdown devices.

Yaskawa Solectria Solar's family of PVI 50/60TL-480 inverters, including standard wireboxes and the rapid-shutdown ready wirebox models, provides flexibility and convenience unmatched in the industry.

Standard Wirebox

- 20A fuses; both polarities
- Not rapid shutdown equipped

Module-Level Rapid Shutdown Wireboxes

- 20A fuses; positive polarity only
- Built-in transmitter for rapid shutdown
- 3 models for compatibility with Tigo, APsmart and NEP shutdown devices

Tigo Enhanced

APsmart ALTENERGY POWER

NEP NORTHERN ELECTRIC

YASKAWA SOLECTRIA SOLAR

Yaskawa Solectria Solar 1-978-683-9700 | Email: inverters@solectria.com | solectria.com
Document No. FLPVI5060TL.01 | 04/12/2021 |

PVI 50TL-480 / PVI 60TL-480 TECHNICAL DATA

SPECIFICATIONS

Inverter Model		PVI 50TL-480	PVI 60TL-480
DC Input	Absolute Maximum Input Voltage	1000 VDC	1000 VDC
	Maximum Power Input Voltage Range (MPPT)	480-850 VDC	540-850 VDC
	Operating Voltage Range (MPPT)	200-950 VDC	200-950 VDC
	Maximum Operating Input Current	108 A (36 A per MPPT)	114 A (38 A per MPPT)
	Number of MPP Trackers	3	3
	Maximum Available PV Current (Isc x 1.25)	204 A (68 A per MPPT)	204 A (68 A per MPPT)
	Maximum PV Power	90 kW (30 kW per MPPT)	90 kW (33 kW per MPPT)
	Start Voltage	330 V	330 V
AC Output	Nominal Output Voltage	480 VAC, 3-Ph/PE/N	480 VAC, 3-Ph/PE/N
	AC Voltage Range (Standard)	-12/+10%	-12/+10%
	PF=1.00 - Real/Apparent Power/Output Current	50 kW / 50 kVA / 60.2 A	60 kW / 60 kVA / 72.3 A
	PF=+/-0.91 - Real/Apparent Power/Output Current	50 kW / 55 kVA / 66.2 A	60 kW / 66 kVA / 79.4 A
	Nominal Output Frequency	60 Hz	60 Hz
	Output Frequency Range	57-63 Hz	57-63 Hz
	Power Factor	Unity, >0.99 (Adjustable 0.8 leading to 0.8 lagging)	Unity, >0.99 (Adjustable 0.8 leading to 0.8 lagging)
	Fault Current Contribution (1 Cycle RMS)	64.1 A	64.1 A
	Total Harmonic Distortion (THD) @ Rated Load	<3%	<3%
	Maximum OCPD Device	110 A	125 A
	AC Surge Protection	Type II MOV, 1240V, 15kA Itm (8/20µ)	
Efficiency	Peak Efficiency	98.8%	98.8%
	CEC Efficiency	98.5%	98.5%
	Tare Loss	< 1 W	< 1 W
Integrated String Combiner	Fused Inputs	15 Fused Positions (5 Positions per MPPT) 20 A Standard (25, 30 A accepted)*	
Temperature	Ambient Temperature Range	-22°F to +140°F (-30°C to +60°C); Derating occurs over +122°F (+50°C)	
	Storage Temperature Range	No low temp minimum to +158°F (+70°C)	
	Relative Humidity (non-condensing)	0-95%	
	Operating Altitude	13,123 ft (4,000 m) Derating occurs from 9,842.5 ft (3,000 m)	
Communications	Modbus Protocol	Proprietary / SunSpec	
	Data Logger Hardware	Standard, Internal	
	SolrenView Web-Based Monitoring Service	Optional	
	Revenue Grade Metering	Optional, External	
	Communication Interface	RS-485 Modbus RTU	
	Remote Firmware Upgrades	Ethernet Network Card required	
	Remote Diagnostics	Ethernet Network Card required	
Features and Protections	Arc-Fault	Standard	
	Smart Grid Features	L/HVRT, L/HFRT, Volt-VAR, Freq-Watt, Volt-Watt, Soft-Start, Soft-Step, Specified-PF	
Testing & Certifications	Safety Listings & Certifications	UL 1741SA-2016, UL1699B, CSA-C22.2 #107.1, IEEE1547a-2014	
	Advanced Grid Support Functionality	Rule 21, UL 1741SA	
	Testing Agency	CSA	
	FCC Compliance	FCC Part 15	
Warranty	Standard Limited Warranty	10 Years	
Enclosure	Acoustic Noise Rating	< 60 dBA @ 1 m at room temperature	
	AC/DC Disconnect	Standard, fully-integrated	
	Mounting Angle**	15 - 90 from horizontal	
	Dimensions (H x W x D)	39.4 in. x 23.6 in. x 10.2 in (1,000 mm x 600 mm x 260 mm)	
	Weight	Inverter: 123.5 lbs (56 kg); Wiring Box: 33 lbs (15 kg)	
	Enclosure Rating and Finish	Type 4X; Polyester Powder Coated Aluminum	

Wirebox Specifications			
Dimensions (H x W x D)	Wirebox	H: 16.7" (424 mm) x W: 23.6" (600 mm) x D: 10.24" (260 mm)	
	Power Head	H: 22.7" (576 mm) x W: 23.6" (600 mm) x D: 10.24" (260 mm)	
	Overall	H: 39.4" (1,000 mm) x W: 23.6" (600 mm) x D: 10.24" (260 mm)	
Wirebox Versions	**PVI-50-60TL-BX-S20:** Standard wirebox	20A fuses, both polarities	MLRSD Compatibility: Not equipped for rapid shutdown
	PVI-50-60TL-BX-R: Tigo RSS transmitter built-in	15A fuses, pos. polarity only	MLRSD Compatibility: Tigo TS4-F and TS4-A-F (ver 6.7+)
	PVI-50-60TL-WB-TGO: Tigo RSS transmitter built-in	20A fuses, both polarities	MLRSD Compatibility: Tigo TS4-F and TS4-A-F (ver 6.7+)
	PVI-50-60TL-WB-APS: APS transmitter built-in	20A fuses, both polarities	MLRSD Compatibility: RSD-S-PLC-A
	PVI-50-60TL-WB-NEP: NEP transmitter built-in	20A fuses, both polarities	MLRSD Compatibility: PVG-1/2/3/4

* Yaskawa Solectria Solar does not supply optional fuses sizes
** Shade cover accessory required for installation of 75° or less

IT'S PERSONAL

YASKAWA SOLECTRIA SOLAR

Yaskawa Solectria Solar 1-978-683-9700 | Email: inverters@solectria.com | solectria.com
Document No. FLPVI5060TL01 | 04/12/2021

Appendix C: Gold Tree Solar Farm Zoning and Torque Tube Coordinates

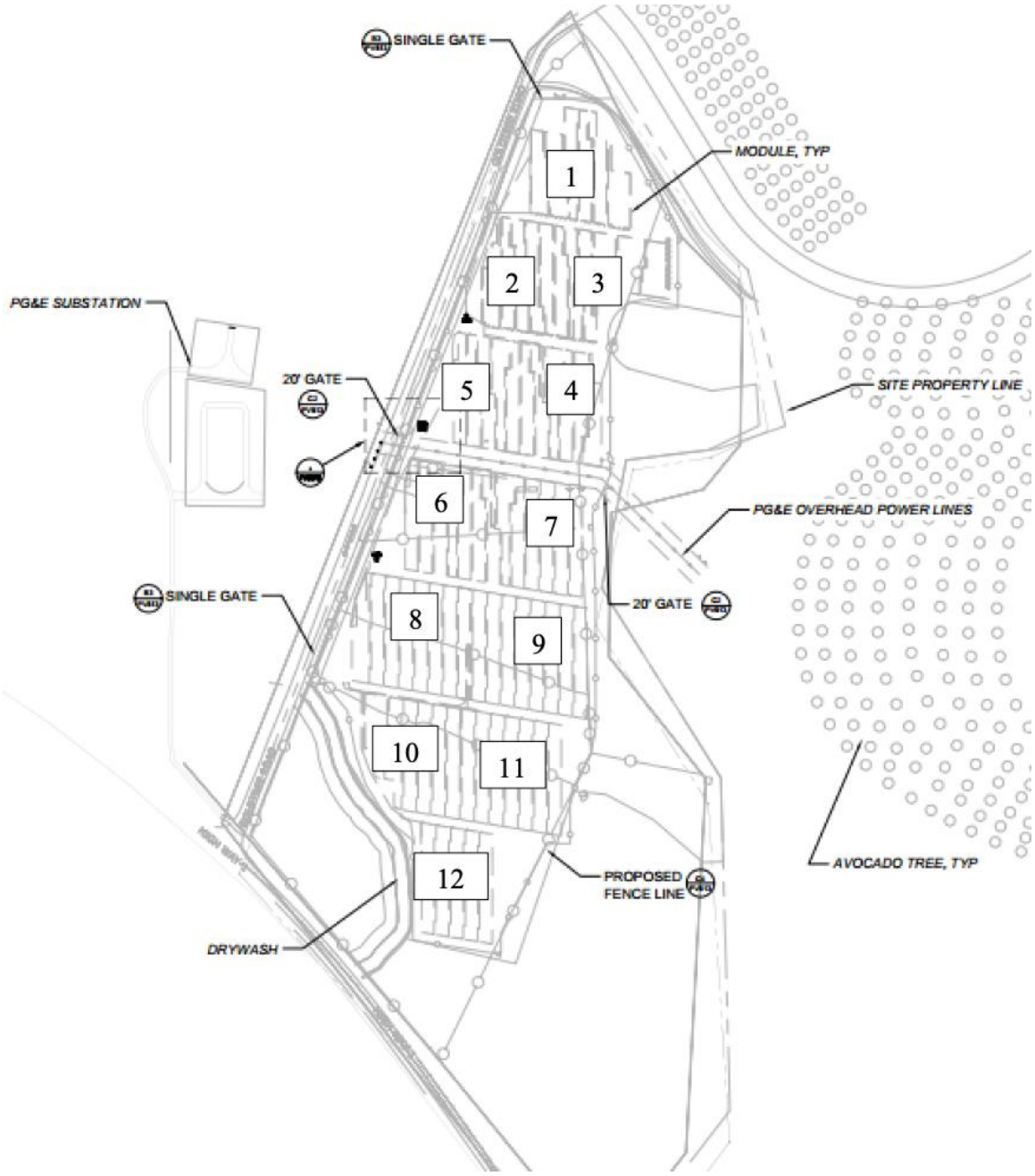

Table C.1 Zone name and number of rows for the Gold Tree Solar Farm

Zone Number	Zone Name	Number of Rows
1	X1	21
2	X2	19
3	X3	20
4	X4	13
5	Y1	18
6	Y2	18
7	Y3	19
8	Y4	20
9	**Z1**	**26**
10	Z2	14
11	Z3	21
12	Z4	15

Table C.2 Coordinates for the torque tubes in Zone Z1. The north end of Row 524 is taken to be the origin and Row 523 is a part of Zone Y4 but shades the first row of Z1 in the afternoons, so its coordinates are also included. All coordinates are in units of meters.

	Torque Tube North End			Torque Tube South End		
Row	x	y	z	x	y	z
523*	-0.450	-3.365	-0.126	76.723	-1.425	-2.906
524	0.000	0.000	0.000	77.176	1.961	-2.743
525	0.451	3.366	0.081	77.624	5.308	-2.655
526	0.897	6.698	0.161	78.077	8.691	-2.592
527	1.351	10.090	0.235	78.525	12.041	-2.499
528	1.799	13.444	0.306	78.973	15.384	-2.436
529	2.250	16.812	0.353	79.425	18.764	-2.354
530	2.695	20.133	0.417	79.881	22.173	-2.294
531	3.149	23.524	0.397	80.326	25.499	-2.289
532	3.595	26.855	0.308	80.780	28.889	-1.890
533	4.044	30.209	0.222	81.232	32.266	-1.988
534	4.494	33.572	0.092	81.682	35.622	-1.805
535	4.948	36.967	-0.002	82.132	38.988	-1.883
536	5.392	40.282	-0.330	82.579	42.323	-1.411
537	5.841	43.638	-0.457	83.035	45.736	-1.524
538	6.293	47.011	-0.771	83.482	49.073	-1.168
539	6.737	50.331	-1.044	83.928	52.407	-1.014
540	7.185	53.676	-1.308	84.379	55.777	-0.773
541	7.641	57.083	-1.706	84.835	59.182	-0.705
542	8.091	60.443	-2.059	85.283	62.524	-0.634
543	8.540	63.803	-2.387	85.733	65.886	-0.521
544	8.990	67.164	-2.795	86.181	69.240	-0.350
545	9.443	70.544	-3.149	86.633	72.615	-0.289
546	9.896	73.929	-3.489	87.081	75.962	-0.221
547	10.343	77.271	-3.890	87.537	79.364	0.064
548	10.796	80.653	-4.164	87.983	82.698	0.250
549	11.244	84.001	-4.480	88.433	86.062	0.486

Table C.3 Coordinates for the torque tubes in Zone Y4. The north end of Row 504 is taken to be the origin. Row 524 is a part of Zone Y4 but shades the last row of Y4 in the mornings, so its coordinates are also included. Rows 501 to 503 are not included as they are not full length, and this analysis does not account for half or three-quarter length rows. All coordinates are in units of meters.

	Torque Tube North End			Torque Tube South End		
Row	x	y	z	x	y	z
504	0.000	0.000	0.000	77.161	2.063	-2.386
505	0.451	3.369	0.101	77.609	5.412	-2.191
506	0.900	6.726	0.402	78.059	8.776	-2.041
507	1.347	10.064	0.527	78.509	12.135	-1.823
508	1.807	13.497	0.783	78.959	15.501	-1.739
509	2.253	16.829	0.905	79.409	18.864	-1.636
510	2.702	20.185	1.016	79.854	22.185	-1.529
511	3.154	23.565	1.114	80.313	25.616	-1.418
512	3.603	26.915	1.243	80.761	28.964	-1.306
513	4.055	30.296	1.365	81.210	32.316	-1.190
514	4.508	33.678	1.485	81.661	35.681	-1.099
515	4.954	37.013	1.559	82.116	39.085	-0.982
516	5.404	40.370	1.670	82.563	42.425	-0.867
517	5.855	43.742	1.767	83.018	45.826	-0.757
518	6.310	47.141	1.950	83.470	49.203	-0.723
519	6.757	50.479	2.052	83.918	52.543	-0.593
520	7.208	53.852	2.187	84.365	55.889	-0.547
521	7.655	57.187	2.283	84.822	59.297	-0.432
522	8.105	60.554	2.414	85.269	62.640	-0.338
523	8.559	63.944	2.505	85.720	66.007	-0.247
524*	9.011	67.319	2.625	86.173	69.393	-0.077

Appendix D: Optimization Routine MATLAB Code

This code shows how the modified tube spacing was optimized

Optimization Routine

Table of Contents

Clear out variables 1
User Inputs 1
Set up Field and Datetimes 2
Begin Preallocation 3
Find Solar Positions and Weather Data 4
Power loop 6
West Optimization 12

Clear out variables

```
clear
close all
clc

Total_Energy = zeros(10,1);
east_tube_spacing_f = zeros(10,1);
```

User Inputs

Set inputs for the code

```
% Set the increment for the modified tube spacing
for spaceinc = 1:10

    % Start Date and Time
    t1 = datetime(2021,12,1,0,0,0);
    % End Date and Time
    t2 = datetime(2021,12,31,23,59,0);
    % Increment in hours
    inc = 10/60;

    % Info for DST vector
    DSTinit = 0;  % DSTinit is 1 if datetimes begins in DST, 0 if in
 standard
    DSTflag = [2021,11,7]; % [Y,M,D; Y,M,D;...] for each DST toggle

    % Input location data
    fileID = fopen('z1_xyz_12_15NSshift.txt');
    sizez1 = [6 27];
    z_1 = fscanf(fileID,'%f',sizez1);
    fclose(fileID);

    % Set number of rows
```

```
num_tubes = 27;

% Modified spacing to adjust onset of backtracking
west_tube_spacing_f = 2.765;
east_tube_spacing_f(spaceinc) = 2.94+.015*spaceinc;
tsfw = west_tube_spacing_f;   % For brevity and maintaining
variable names
tsfe = east_tube_spacing_f(spaceinc);

% Set panel width and their spacing between cells
panel_offset = .127;
panel_width = 1.9558;
pw = panel_width;       % For brevity and maintaining variable
names

% Set field location
% Cal Poly Solar Farm Location
Location.latitude = 35.317;    % [arc-degrees] latitude
Location.longitude = -120.689; % [arc-degrees] longitude
Location.altitude = 100;       % altitude
TZ = -8;         % [hrs] offset from UTC, during standard time

% End User Input
```

Set up Field and Datetimes

```
disp("Working on " + spaceinc);

% set x,y,z of both ends of torque tubes
xt1 = z_1(1,:);
yt1 = z_1(2,:);
zt1 = z_1(3,:);
xt2 = z_1(4,:);
yt2 = z_1(5,:);
zt2 = z_1(6,:);

% set up datetimes
t = t1:hours(inc):t2;
datestring = datestr(t,'mm/dd/yyyy HH:MM AM');
datetimes = cellstr(datestring);
daydim = length(datetimes);

disp(" ");
disp("Number of date and time inputs: " + daydim);
disp(" ");
```

```
Working on 1

Number of date and time inputs: 4464


Working on 2
```

```
Number of date and time inputs: 4464


Working on 3

Number of date and time inputs: 4464


Working on 4

Number of date and time inputs: 4464


Working on 5

Number of date and time inputs: 4464


Working on 6

Number of date and time inputs: 4464


Working on 7

Number of date and time inputs: 4464


Working on 8

Number of date and time inputs: 4464


Working on 9

Number of date and time inputs: 4464


Working on 10

Number of date and time inputs: 4464
```

Begin Preallocation

```
DSTflagNum = zeros(size(DSTflag,1),1);
DST = NaN(daydim,1);
theta = zeros(daydim,1);
sundown = zeros(daydim,1);
cs = zeros(4,3,num_tubes);
pC = zeros(4,3,num_tubes);
pS = zeros(4,3,num_tubes);
lgth =zeros(num_tubes-1,daydim);
```

```
   hght =zeros(num_tubes-1,daydim);
   Power = zeros(num_tubes,daydim);
   Total_Power = zeros(daydim,1);
   % End Preallocation
```

Find Solar Positions and Weather Data

Determines whether the daylight savings switches and finds the solar position and weather conditions including wind speed, POA irradiance, and ambient temperature. Then finds the cell temperature and sets up the four corners for each row.

```
   % Create DST vector
   zones = size(DSTflag,1) + 1;      % Number of time zones
   for i = 1:(zones-1)               % Convert to numerical
representation
       DSTflagNum(i) = datenum(DSTflag(i,:));
   end

   % Counter setup
   zone = 1;
   now = datenum(datetimes(1));
   DSTindex = 1;
   DSTnow = DSTinit;

   while zone < zones                % While we are not past the last
DST flag,
       while now < DSTflagNum(zone) % and while we are still in the
same zone,
           DST(DSTindex) = DSTnow;  % DST is the current value.
           DSTindex = DSTindex + 1; % We move to the next value of
DST
           now = now...             % as we increment time to catch
up.
               + datenum(datetimes(DSTindex))...
               - datenum(datetimes(DSTindex-1));
       end
       DSTnow = mod(DSTnow+1,2);    % When the zone ends, current DST
toggles
       zone = zone + 1;             % as we move to the next zone.
   end

   for i = DSTindex:daydim          % Once we pass the last DST flag,
       DST(i) = DSTnow;             % the rest of DST is the current
value.
   end


   % Calculate solar positions
   % Convert datetimes into a time structure
   Time = pvl_maketimestruct(datenum(datetimes), TZ+DSTnow); % -7
DLS, -8 standard
   [SunAz, ~, ApparentSunEl, ~]=pvl_ephemeris(Time, Location);
```

```
    % define light ray vectors based on sun position
    ur = [-cos(ApparentSunEl*pi/180).*cos((SunAz)*pi/180) ...
        cos(ApparentSunEl*pi/180).*sin((SunAz)*pi/180) ...
        sin(ApparentSunEl*pi/180)];

    % Check for times outside sunrise and sunset
    for i = 1:daydim
        if ApparentSunEl(i)<0
            %disp(datetimes(i)+ " is either before sunrise or after
sunset.");
            sundown(i)=1;
        end
    end

    % Get local ambient temperature data
    T_amodel = sloTempM(datetimes,DST);

    % Use actual data for ambient temperature
    % fileID = fopen('116Tempdata.txt');
    % size = [1 288];
    % T_a = fscanf(fileID,'%f',size);
    % fclose(fileID);

    T_a = T_amodel;

    % Use actual data for wind speed
    % fileID = fopen('116Winddata.txt');
    % size = [1 288];
    % v_wind = fscanf(fileID,'%f',size);
    % fclose(fileID);

    % Get local wind speed data
    v_wind = sloWind(datetimes,DST);

    % Calculate panel tilt angles
    dsa = atan(ur(:,3)./ur(:,2));      % Direct sun angle
    dsa(dsa < 0) = dsa(dsa < 0) + pi;  % Flip panel around if negative
angle

    %deterimine if backtracking or tracking
    for i = 1:daydim
        %if time is before noon, or after noon
        if ApparentSunEl(i)>0
            if SunAz(i) < 180
                sba = asin(pw/tsfe);
            else
                sba = asin(pw/tsfw);          % Start-of-backtracking
angle
            end
            if isnan(dsa(i))
                theta(i)=(-52+90)*pi/180;
            % Direct tracking region
            elseif (dsa(i) > sba) && (dsa(i) < pi-sba)
                theta(i) = dsa(i);
```

```
            % Backtracking region
            else
                if dsa(i) < pi/2
                    angle = dsa(i);                 % morning
                    theta(i) = pi/2 + (angle - asin(tsfe/
pw*sin(angle)));
                else
                    angle = pi - dsa(i);            % afternoon
                    theta(i) = pi/2 - (angle - asin(tsfw/
pw*sin(angle)));
                end
            end
        else
            theta(i) = (-55+90)*pi/180; % stow away angle
        end
    end

    theta_deg = theta * 180/pi;
    theta_GT = theta_deg - 90; % Gold Tree Def for Tracker Angle


    % Calculate POA irradiance
    [POA] = POAgen(Location, abs(theta_GT), datetimes, DST);

    % Use actual data for :OA irradiance
    % fileID = fopen('116POAdata.txt');
    % size = [1 288];
    % [POA] = fscanf(fileID,'%f',size);
    % fclose(fileID);

    % Calculate Cell temperature
    T_cell = celltemp(T_a,POA,v_wind);

    % Define offsets for start and end of panels relative to tubes
    offsetN = 0.7;
    offsetS = 0.65;

    % Find torque tube vectors and lengths
    tubevecs = [xt2'-xt1', yt2'-yt1', zt2'-zt1'];
    tubelengths = sqrt(dot(tubevecs,tubevecs,2)) - offsetN - offsetS;

    % Define panel corners in local torque tube coordinate system
    for i = 1:num_tubes
        cs(:,:,i) = [panel_offset  -panel_width/2
 offsetN;
            panel_offset  -panel_width/2  tubelengths(i) + offsetN;
            panel_offset   panel_width/2  tubelengths(i) + offsetN;
            panel_offset   panel_width/2                 offsetN];
    end
```

Power loop

Calculate shading and power output for each datetime

```
   for ntime = 1:daydim

       %disp("Working on " + datetimes(ntime) + "...");
       if sundown(ntime) == 0
           for i = 1:num_tubes
               % Tilt panels about z-axis in torque tube coordinates
               Rz = [ cos(theta(ntime)) sin(theta(ntime)) 0;
                   -sin(theta(ntime)) cos(theta(ntime)) 0;
                   0                  0                 1];
               cz = cs(:,:,i) * Rz;

               % Convert torque tube coordinates to cardinal
coordinates
               pC0 = sol2carRH(cz,tubevecs(i,:));  % Happens to be the
appr. op.

               % Translate panel to global position
               for j = 1:4
                   pC(j,1,i) = pC0(j,1) + xt1(i);
                   pC(j,2,i) = pC0(j,2) + yt1(i);
                   pC(j,3,i) = pC0(j,3) + zt1(i);
               end

               % Convert to solar coordinate system (ur is z-axis)
               pS(:,:,i) = car2solRH(pC(:,:,i),ur(ntime,:));
           end
           % Direction of shade projection and order of panel shade
analysis
           if SunAz(ntime) < 180
               ft = num_tubes;
               lt = 1;
               dir = -1;
           else
               ft = 1;
               lt = num_tubes;
               dir = 1;
           end

           % Preallocate for shade points for visualization purposes
           end1C = NaN(num_tubes,3);
           end2C = NaN(num_tubes,3);
           end1S3D = NaN(num_tubes,3);
           end2S3D = NaN(num_tubes,3);

           for k = ft:dir:lt
               % Find normal unit vector to panel in cardinal
coordinates
               npC = cross((pC(1,:,k)-pC(2,:,k)), ...
                   (pC(3,:,k)-pC(2,:,k)));
               npCu = npC / sqrt(dot(npC,npC));

               if POA(ntime) > 0
                   if k == ft
                       % Zero shade on panel closest to the sun
```

```
                sy_1 = 0;
                sy_2 = 0;
                sx_1 = 0;
                sx_2 = 1;

            else
                % Corners: b = Bottom, t = Top, l = Left, r =
Right
                % Panels: F = Front, B = Back
                if dir == 1
                    tlF = pS(1,1:2,k-dir);
                    trF = pS(2,1:2,k-dir);
                    brF = pS(3,1:2,k-dir);
                    blF = pS(4,1:2,k-dir);
                    tlB = pS(1,1:2,k);
                    trB = pS(2,1:2,k);
                    brB = pS(3,1:2,k);
                    blB = pS(4,1:2,k);
                else
                    tlF = pS(3,1:2,k-dir);
                    trF = pS(4,1:2,k-dir);
                    brF = pS(1,1:2,k-dir);
                    blF = pS(2,1:2,k-dir);
                    tlB = pS(3,1:2,k);
                    trB = pS(4,1:2,k);
                    brB = pS(1,1:2,k);
                    blB = pS(2,1:2,k);
                    reordera=pC(1,:,k);
                    reorderb=pC(2,:,k);
                    reorderc=pC(3,:,k);
                    reorderd=pC(4,:,k);
                    pC(3,:,k)=reordera;
                    pC(4,:,k)=reorderb;
                    pC(1,:,k)=reorderc;
                    pC(2,:,k)=reorderd;
                end

                % Find shade and panel edge intersections,
NaNs if DNE
                txl = segmentInt2D([tlF;trF;tlB;blB]);
                txr = segmentInt2D([tlF;trF;trB;brB]);
                txb = segmentInt2D([tlF;trF;blB;brB]);
                txt = segmentInt2D([tlF;trF;tlB;trB]);

                % Determine if intersections exist
                txlExists = isfinite(txl(1));
                txrExists = isfinite(txr(1));
                txbExists = isfinite(txb(1));
                txtExists = isfinite(txt(1));

                % Shade case index
                shadeCase = 8*txtExists + 4*txbExists ...
                    + 2*txlExists ...
                    + 1*txrExists;
```

```
                        % Find shade endpoints in 2D solar coordinate
xy-plane
                        % 1's mean txb, txl, txr exist respectively
                        switch shadeCase
                            case bin2dec('0000')
                                if
isfinite(segmentInt2D([tlF;blF;blB;brB]))
                                    end1S = tlF;
                                    end2S = trF;
                                else
                                    end1S = [NaN NaN];
                                    end2S = [NaN NaN];
                                end
                            case bin2dec('0001')
                                end1S = tlF;
                                end2S = txr;
                            case bin2dec('0010')
                                end1S = txl;
                                end2S = trF;
                            case bin2dec('0011')
                                end1S = txl;
                                end2S = txr;
                            case bin2dec('0100')
                                if
isfinite(segmentInt2D([tlF;blF;blB;brB]))
                                    end1S = tlF;
                                    end2S = txb;
                                else
                                    end1S = txb;
                                    end2S = trF;
                                end
                            case bin2dec('0101')
                                end1S = txb;
                                end2S = txr;
                            case bin2dec('0110')
                                end1S = txl;
                                end2S = txb;
                            case bin2dec('1100')
                                end1S = txt;
                                end2S = txb;
                            case bin2dec('1010')
                                end1S = txl;
                                end2S = txt;
                            case bin2dec('1001')
                                end1S = txt;
                                end2S = txr;
                        end

                        if isnan(end1S(1))
                            % Zero shade input for power subroutine
                            sy_1 = 0;
                            sy_2 = 0;
                            sx_1 = 0;
```

```
                        sx_2 = 1;
                    else
                        % Find rear panel normal vector in solar
coordinates
                        npS = car2solRH(npC,ur(ntime,:));

                        % Add z-coordinate of shade points in
solar coordinates
                        end1S3D(k,:) = addz(end1S,npS,pS(1,:,k));
                        end2S3D(k,:) = addz(end2S,npS,pS(1,:,k));

                        % Convert back to cardinal coordinates
                        end1C(k,:) =
sol2carRH(end1S3D(k,:),ur(ntime,:));
                        end2C(k,:) =
sol2carRH(end2S3D(k,:),ur(ntime,:));

                        % Define local panel coordinate system
axes
                        PxC = pC(3,:,k) - pC(4,:,k);
                        PyC = pC(1,:,k) - pC(4,:,k);

                        % Translate to match panel and cardinal
system origins
                        end1C0 = end1C(k,:) - pC(4,:,k);
                        end2C0 = end2C(k,:) - pC(4,:,k);

                        % Convert to local panel coordinate system
                        end1P0 = car2arbRH(end1C0,PxC,PyC);
                        end2P0 = car2arbRH(end2C0,PxC,PyC);

                        % Find power subroutine inputs
                        sy_1 = min(end1P0(2),end2P0(2));
                        sy_2 = max(end1P0(2),end2P0(2));
                        sx_1 = min(end1P0(1),end2P0(1));
                        sx_2 = max(end1P0(1),end2P0(1));
                    end
                end
                lgth(k,ntime) = (sx_2-sx_1)*39.3701;
                hght(k,ntime) = sy_2*39.3701;
                %Call power subroutine
                if k==ft
                else
                    Power(k,ntime) = power_sub_11_8(sy_1, sy_2,
sx_1, sx_2,...
                        POA(ntime), T_cell(ntime))/1000;
                end
                if Power(k,ntime)>20.3
                    Power(k,ntime)=20.3;
                end
            else
                %disp("Sun is below the plane of the panel at this
time.");
            end
```

```
            end
        else
            for i = 1:num_tubes
                theta(ntime)=(-52+90)*pi/180;
                % Tilt panels about z-axis in torque tube coordinates
                Rz = [ cos(theta(ntime)) sin(theta(ntime)) 0;
                    -sin(theta(ntime)) cos(theta(ntime)) 0;
                    0                  0                 1];
                cz = cs(:,:,i) * Rz;

                % Convert torque tube coordinates to cardinal
 coordinates
                pC0 = sol2carRH(cz,tubevecs(i,:));  % Happens to be the
 appr. op.

                % Translate panel to global position
                for j = 1:4
                    pC(j,1,i) = pC0(j,1) + xt1(i);
                    pC(j,2,i) = pC0(j,2) + yt1(i);
                    pC(j,3,i) = pC0(j,3) + zt1(i);
                end
            end
        end
        Total_Power(ntime) = sum(Power(:,ntime));
        %TotalEnergy = Total_Power(ntime)*5/60
        %if Total_Power(ntime)>61
        %    Total_Power(ntime) = 61;
        %end
    end
    Total_Energy(spaceinc) = sum(Total_Power*inc);

end


disp(" ");
disp("Total Energy =");
disp(" ");
disp(Total_Energy);

% disp("NOTE: The program in its current state assumes");
% disp("that the panel closest to the sun is unshaded.");
```

```
Total Energy =

   1.0e+04 *
    7.8407
    7.8416
    7.8423
    7.8421
    7.8416
    7.8404
    7.8383
    7.8359
```

```
    7.8330
    7.8289
```

West Optimization

```
close all
tsfwopt = load('west_tube_spacing_opt.mat');
west_tube_spacing_f = tsfwopt.west_tube_spacing_f;

% Load optimization energy outputs for each month
JanEnergyWestOpt = load('JanEnergyWestOpt.mat');
FebEnergyWestOpt = load('FebEnergyWestOpt.mat');
MarEnergyWestOpt = load('MarEnergyWestOpt.mat','-mat');
AprEnergyWestOpt = load('AprEnergyWestOpt.mat','-mat');
MayEnergyWestOpt = load('MayEnergyWestOpt.mat','-mat');
JuneEnergyWestOpt = load('JuneEnergyWestOpt.mat','-mat');
JulyEnergyWestOpt = load('JulyEnergyWestOpt.mat','-mat');
AugEnergyWestOpt = load('AugEnergyWestOpt.mat','-mat');
SepEnergyWestOpt = load('SepEnergyWestOpt.mat','-mat');
OctEnergyWestOpt = load('OctEnergyWestOpt.mat','-mat');
NovEnergyWestOpt = load('NovEnergyWestOpt.mat','-mat');
DecEnergyWestOpt = load('DecEnergyWestOpt.mat','-mat');


% Assign max energy values and the nominal 11ft values for each month
janmaxenergy = 94206.3237965049;
jan11ft = 80709.4068898587;
febmaxenergy = 109722.851679201;
feb11ft = 94712.8927017896;
marmaxenergy = 145930.100421123;
mar11ft = 126749.524729210;
aprmaxenergy = 158540.167925848;
apr11ft = 137612.056929958;
maymaxenergy = 177452.735338266;
may11ft = 154073.523466483;
junemaxenergy = 176669.289708890;
june11ft = 153988.765815251;
julymaxenergy = 180238.363069941;
july11ft = 156603.353121365;
augmaxenergy = 169734.491440181;
aug11ft = 146928.960718614;
sepmaxenergy = 149456.291850034;
sep11ft = 129201.536374660;
octmaxenergy = 125004.848154081;
oct11ft = 108517.763800215;
novmaxenergy = 97937.0467732672;
nov11ft = 83932.5497348241;
decmaxenergy = 86052.0998947034;
dec11ft = 73412.1268026416;

% Create figure of optimizations for January through June
figure
% Plot energy vs tube spacing in feet
```

```
plot(west_tube_spacing_f*3.28084,JanEnergyWestOpt.Total_Energy/
janmaxenergy,'b','LineWidth',2)
hold on
plot(west_tube_spacing_f*3.28084,FebEnergyWestOpt.Total_Energy/
febmaxenergy,'g','LineWidth',2)
plot(west_tube_spacing_f*3.28084,MarEnergyWestOpt.Total_Energy/
marmaxenergy,'c','LineWidth',2)
plot(west_tube_spacing_f*3.28084,AprEnergyWestOpt.Total_Energy/
aprmaxenergy,'m','LineWidth',2)
plot(west_tube_spacing_f*3.28084,MayEnergyWestOpt.Total_Energy/
maymaxenergy,'k','LineWidth',2)
plot(west_tube_spacing_f*3.28084,JuneEnergyWestOpt.Total_Energy/
junemaxenergy,'r','LineWidth',2)

% plot nominal values and max energy point and label with tube spacing
% value in feet
plot([8.4,9.6],[jan11ft/janmaxenergy,jan11ft/janmaxenergy], '--
b','LineWidth',2)
plot(west_tube_spacing_f(11)*3.28084,max(JanEnergyWestOpt.Total_Energy)/
janmaxenergy,'.b',...
    'MarkerSize',15,'HandleVisibility','off')
text(west_tube_spacing_f(11)*3.28084-.1,max(JanEnergyWestOpt.Total_Energy)/
janmaxenergy-.002,...
    '9.07 ft','Color','b')
plot([8.4,9.6],[feb11ft/febmaxenergy,feb11ft/febmaxenergy], '--
g','LineWidth',2)
plot(west_tube_spacing_f(12)*3.28084,max(FebEnergyWestOpt.Total_Energy)/
febmaxenergy,'.g',...
    'MarkerSize',15,'HandleVisibility','off')
text(west_tube_spacing_f(12)*3.28084-.1,max(FebEnergyWestOpt.Total_Energy)/
febmaxenergy-.002,...
    '9.12 ft','Color','g')
plot([8.4,9.6],[mar11ft/marmaxenergy,mar11ft/marmaxenergy], '--
c','LineWidth',2)
plot(west_tube_spacing_f(12)*3.28084,max(MarEnergyWestOpt.Total_Energy)/
marmaxenergy,'.c',...
    'MarkerSize',18,'HandleVisibility','off')
text(west_tube_spacing_f(12)*3.28084-.05,max(MarEnergyWestOpt.Total_Energy)/
marmaxenergy+.002,...
    '9.12 ft','Color','c')
plot([8.4,9.6],[apr11ft/aprmaxenergy,apr11ft/aprmaxenergy], '--
m','LineWidth',2)
plot(west_tube_spacing_f(12)*3.28084,max(AprEnergyWestOpt.Total_Energy)/
aprmaxenergy,'.m',...
    'MarkerSize',12,'HandleVisibility','off')
text(west_tube_spacing_f(12)*3.28084-.05,max(AprEnergyWestOpt.Total_Energy)/
aprmaxenergy-.002,...
    '9.12 ft','Color','m')
plot([8.4,9.6],[may11ft/maymaxenergy,may11ft/maymaxenergy], '--
k','LineWidth',2)
plot(west_tube_spacing_f(13)*3.28084,max(MayEnergyWestOpt.Total_Energy)/
maymaxenergy,'.k',...
    'MarkerSize',15,'HandleVisibility','off')
```

```
text(west_tube_spacing_f(13)*3.28084,max(MayEnergyWestOpt.Total_Energy)/
maymaxenergy-.002,...
    '9.17 ft','Color','k')
plot([8.4,9.6],[june11ft/junemaxenergy,june11ft/junemaxenergy], '--
r','LineWidth',2)
plot(west_tube_spacing_f(14)*3.28084,max(JuneEnergyWestOpt.Total_Energy/
junemaxenergy),'.r',...
    'HandleVisibility','off','MarkerSize',15)
text(west_tube_spacing_f(14)*3.28084+.02,max(JuneEnergyWestOpt.Total_Energy)/
junemaxenergy+.002,...
    '9.22 ft','Color','r')

% Create legend and titles
legend('January','February','March','April','May','June','Jan
 Nominal','Feb Nominal',...
    'Mar Nominal','Apr Nominal','May Nominal','June
 Nominal','Location','Southeast')
xlabel('West Tube Spacing (ft)')
ylabel('Normalized Monthly Energy (kWh)')
title('January through June')
print(1, '-dpng', 'JanJunoptzoomfinenormalized', '-r500')


% Create figure of optimizations for July through December
figure
% Plot energy vs tube spacing in feet
plot(west_tube_spacing_f*3.28084,JulyEnergyWestOpt.Total_Energy/
julymaxenergy,'b','LineWidth',2)
hold on
plot(west_tube_spacing_f*3.28084,AugEnergyWestOpt.Total_Energy/
augmaxenergy,'g','LineWidth',2)
plot(west_tube_spacing_f*3.28084,SepEnergyWestOpt.Total_Energy/
sepmaxenergy,'c','LineWidth',2)
plot(west_tube_spacing_f*3.28084,OctEnergyWestOpt.Total_Energy/
octmaxenergy,'m','LineWidth',2)
plot(west_tube_spacing_f*3.28084,NovEnergyWestOpt.Total_Energy/
novmaxenergy,'k','LineWidth',2)
plot(west_tube_spacing_f*3.28084,DecEnergyWestOpt.Total_Energy/
decmaxenergy,'r','LineWidth',2)

% plot nominal values and max energy point and label with tube spacing
% value in feet
plot([8.4,9.6],[july11ft/julymaxenergy,july11ft/julymaxenergy], '--
b','LineWidth',2)
plot(west_tube_spacing_f(13)*3.28084,max(JulyEnergyWestOpt.Total_Energy)/
julymaxenergy,'.b',...
    'MarkerSize',15,'HandleVisibility','off')
text(west_tube_spacing_f(13)*3.28084-.1,max(JulyEnergyWestOpt.Total_Energy)/
julymaxenergy+.001,...
    '9.17 ft','Color','b')
plot([8.4,9.6],[aug11ft/augmaxenergy,aug11ft/augmaxenergy], '--
g','LineWidth',2)
plot(west_tube_spacing_f(12)*3.28084,max(AugEnergyWestOpt.Total_Energy)/
augmaxenergy,'.g',...
```

```
    'MarkerSize',15,'HandleVisibility','off')
text(west_tube_spacing_f(12)*3.28084+.03,max(AugEnergyWestOpt.Total_Energy)/
augmaxenergy-.002,...
    '9.12 ft','Color','g')
plot([8.4,9.6],[sep11ft/sepmaxenergy,sep11ft/sepmaxenergy], '--
c','LineWidth',2)
plot(west_tube_spacing_f(12)*3.28084,max(SepEnergyWestOpt.Total_Energy)/
sepmaxenergy,'.c',...
    'MarkerSize',18,'HandleVisibility','off')
text(west_tube_spacing_f(12)*3.28084-.1,max(SepEnergyWestOpt.Total_Energy)/
sepmaxenergy-.002,...
    '9.12 ft','Color','c')
plot([8.4,9.6],[oct11ft/octmaxenergy,oct11ft/octmaxenergy], '--
m','LineWidth',2)
plot(west_tube_spacing_f(13)*3.28084,max(OctEnergyWestOpt.Total_Energy)/
octmaxenergy,'.m',...
    'MarkerSize',12,'HandleVisibility','off')
text(west_tube_spacing_f(13)*3.28084+.01,max(OctEnergyWestOpt.Total_Energy)/
octmaxenergy+.002,...
    '9.17 ft','Color','m')
plot([8.4,9.6],[nov11ft/novmaxenergy,nov11ft/novmaxenergy], '--
k','LineWidth',2)
plot(west_tube_spacing_f(11)*3.28084,max(NovEnergyWestOpt.Total_Energy)/
novmaxenergy,'.k',...
    'MarkerSize',15,'HandleVisibility','off')
text(west_tube_spacing_f(11)*3.28084,max(NovEnergyWestOpt.Total_Energy)/
novmaxenergy+.002,...
    '9.07 ft','Color','k')
plot([8.4,9.6],[dec11ft/decmaxenergy,dec11ft/decmaxenergy], '--
r','LineWidth',2)
plot(west_tube_spacing_f(11)*3.28084,max(DecEnergyWestOpt.Total_Energy/
decmaxenergy),'.r',...
    'HandleVisibility','off','MarkerSize',15)
text(west_tube_spacing_f(11)*3.28084+.02,max(DecEnergyWestOpt.Total_Energy)/
decmaxenergy-.002,...
    '9.07 ft','Color','r')

% Create legend and titles
legend('July','August','September','October','November','December',...
    'July Nominal','Aug Nominal','Sep Nominal','Oct Nominal','Nov
 Nominal',...
    'Dec Nominal','Location','Southeast')
xlabel('West Tube Spacing (ft)')
ylabel('Normalized Monthly Energy (kWh)')
title('July through December')
print(2, '-dpng', 'JulyDecoptzoomfinenormalized', '-r500')
```

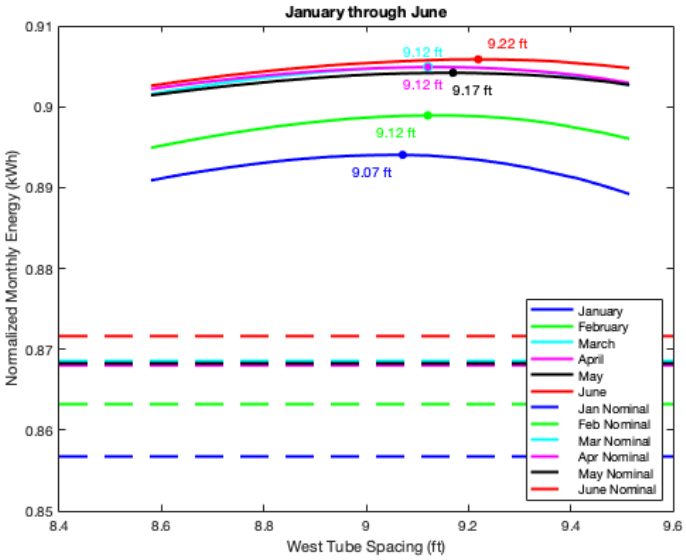
January through June
Normalized Monthly Energy (kWh)
West Tube Spacing (ft)
9.22 ft
9.12 ft
9.12 ft
9.17 ft
9.12 ft
9.07 ft
January
February
March
April
May
June
Jan Nominal
Feb Nominal
Mar Nominal
Apr Nominal
May Nominal
June Nominal

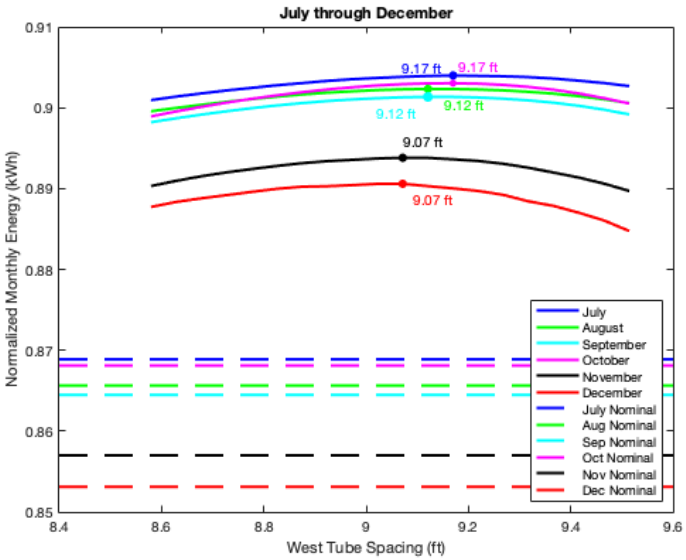
July through December
Normalized Monthly Energy (kWh)
West Tube Spacing (ft)
9.17 ft
9.17 ft
9.12 ft
9.12 ft
9.07 ft
9.07 ft
July
August
September
October
November
December
July Nominal
Aug Nominal
Sep Nominal
Oct Nominal
Nov Nominal
Dec Nominal